CHEMISTRY
A EUROPEAN JOURNAL

DOI: 10.1002/chem.200800539

Spectroelectrochemical and Computational Studies on the Mechanism of Hypoxia Selectivity of Copper Radiopharmaceuticals

Jason P. Holland,*[a] Peter J. Barnard,[a] David Collison,[b] Jonathan R. Dilworth,*[a] Ruth Edge,[b] Jennifer C. Green,*[a] and Eric J. L. McInnes[b]

Abstract: Detailed chemical, spectroelectrochemical and computational studies have been used to investigate the mechanism of hypoxia selectivity of a range of copper radiopharmaceuticals. A revised mechanism involving a delicate balance between cellular uptake, intracellular reduction, reoxidation, protonation and ligand dissociation is proposed. This mechanism accounts for observed differences in the reported cellular uptake and washout of related copper bis(thiosemicarbazonato) complexes. Three copper and zinc complexes have been characterised by X-ray crystallography and the redox chemistry of a series of copper complexes has been investigated by using electronic absorption and EPR spectroelectrochemistry. Time-dependent density functional theory (TD-DFT) calculations have also been used to probe the electronic structures of intermediate species and assign the electronic absorption spectra. DFT calculations also show that one-electron oxidation is ligand-based, leading to the formation of cationic triplet species. In the absence of protons, metal-centred one-electron reduction gives the reduced anionic copper(I) species, $[Cu^{I}ATSM]^{-}$, and for the first time it is shown that molecular oxygen can reoxidise this anion to give the neutral, lipophilic parent complexes, which can wash out of cells. The electrochemistry is pH dependent and in the presence of stronger acids both chemical and electrochemical reduction leads to quantitative and rapid dissociation of copper(I) ions from the mono- or diprotonated complexes, $[Cu^{I}ATSMH]$ and $[Cu^{I}ATSMH_2]^{+}$. In addition, a range of protonated intermediate species have been identified at lower acid concentrations. The one-electron reduction potential, rate of reoxidation of the copper(I) anionic species and ease of protonation are dependent on the structure of the ligand, which also governs their observed behaviour in vivo.

Keywords: density functional calculations · hypoxia · mechanistic studies · radiopharmaceuticals · spectroelectrochemistry

Introduction

Oxygen is of fundamental importance for all tissues, which includes solid tumours.[1] All aspects of the cellular growth cycle, from the pathways and reaction rates of metabolism to cell mitosis and apoptosis, are influenced by the amount of oxygen present within the tissue. As a consequence, tissue oxygen tension in vivo is highly regulated and the mechanisms that operate to maintain an adequate supply of oxygen to the required areas involve proteins expressed by over 200 genes.[2]

Reduced oxygenation of tissue, also known as hypoxia, is a common feature of several diseases, such as stroke, heart disease and certain types of cancer.[3–5] For a patient suffering from cancer there are three primary courses of treatment available to the clinician: surgery, radiation therapy or chemotherapy. However, since the pioneering work of Gray et al. in 1953,[6] it has been known that hypoxia confers resistance to both ionising radiation and chemotherapy, which

[a] Dr. J. P. Holland, Dr. P. J. Barnard, Prof. J. R. Dilworth, Prof. J. C. Green
Chemistry Research Laboratory, Department of Chemistry
University of Oxford, 12 Mansfield Road
Oxford, OX1 3TA (UK)
Fax: (+44) 1865-272690
E-mail: jason.holland@chem.ox.ac.uk
jon.dilworth@chem.ox.ac.uk
jennifer.green@chem.ox.ac.uk

[b] Prof. D. Collison, Dr. R. Edge, Prof. E. J. L. McInnes
Chemistry, EPSRC National Service for EPR Spectroscopy
School of Chemistry, The University of Manchester
Oxford Road, Manchester, M13 9PL (UK)

Supporting information for this article is available on the WWW under http://www.chemeurj.org/ or from the author. It contains X-ray crystallographic data for complexes **7–9** (CIF format), Figures 6 to 9, 11, and 13 to 16 in colour, full experimental details along with DFT optimised Cartesian coordinates and MO diagrams and additional details of the cyclic voltammetry, UV/Vis SEC and EPR experiments.

reduces the efficacy of these forms of treatment and with it the prognosis for patient survival.[3,7] Early identification of the location and extent of hypoxia is potentially important for effective clinical management of these and other diseases.[4]

Molecular imaging techniques, such as positron emission tomography (PET) and single photon emission computerised tomography (SPECT), and the importance of developing imaging agents capable of delineating hypoxia have been reviewed extensively.[8–13] Normal tissue shows a typical Gaussian distribution of oxygen tensions with values of pO_2 ranging from 20 to 80 mm Hg, with a median value around 50 mm Hg, and none less than 10 mm Hg.[14] Tumours exhibit much lower levels of oxygenation and a median value of pO_2 around 10 mm Hg has been identified by Brizel et al. as the point at which resistance to ionising radiation and chemotherapy starts to develop.[15] Full resistance occurs in tissue in which pO_2 is <0.5 mm Hg, and crucially, tumour oxygenation was found to correlate with the probability of disease-free patient survival after a standard course of radiotherapy.[3]

The development of PET imaging agents as non-invasive, hypoxia-selective markers has recently been the subject of intense research.[12,13,16,17] The chemical diversity of inorganic and organometallic compounds means that an ever increasing number of potential radiopharmaceuticals are being developed around metallic elements such as copper, gallium and technetium.[18] Biodistribution studies on several promising hypoxia-selective compounds have also been reported. These compounds include the 2-nitroimidazoles, pimonidazole, ^{18}F-labelled 2-(2-nitro-1*H*-imidazol-1-yl)-*N*-(2,2,3,3,3-pentafluoropropyl)acetamide ([^{18}F]-EF5)[19] and [^{18}F]-fluoromisonidazole ([^{18}F]-FMISO),[20] cytotoxin tirapazamine (TZP),[21,22] and the technetium complex of the ligand HL91 (^{99m}Tc-HL91, HL91 = 2,2′-(1,4-diaminobutane)bis(2-methyl-3-butanone)dioxime)[23] used as a SPECT imaging agent. In addition, a versatile class of complexes for potential use as both imaging and radiotherapeutic agents known as copper(II)–bis(thiosemicarbazonato) complexes have been developed.[24]

In 1997, Fujibayashi et al. first observed hypoxia-selective tissue uptake of the copper(II) complex of the diacetyl bis(4-*N*-methyl-3-thiosemicarbazonato) ligand, [^{62}Cu^{II}ATSM], in ex vivo ischemic, perfused, isolated rat heart models.[25] Following successful preclinical trials, the copper-64 complex [^{64}Cu^{II}ATSM] has been approved for use in multi-centre clinical trials by the United States Federal Drug Administration (US-FDA) as an "Investigational New Drug" (IND 62,675) for imaging patients with cervical cancer.[26] [Cu^{II}ATSM] (**1**) has emerged as the leading copper-based radiopharmaceutical targeting tumour hypoxia, and further human trials to image tumour hypoxia are currently underway in the US and Europe.[27–34] In addition, Obata et al. have also demonstrated the potential for [^{64}Cu^{II}ATSM] to be used as a radiotherapeutic agent.[35]

Despite numerous articles describing in vivo characterisation, PET imaging and structure–activity relationship (SAR) studies on various copper(II)–bis(thiosemicarbazonato) complexes, the mechanism of cellular uptake, localisation and trapping within normoxic and hypoxic tissue remain uncertain.[25,36–40] Each process is likely to be dependent on several factors, which include the nature of the copper(II) complex, tissue phenotype and local tissue oxygen tension. Two main theories on the mechanism of hypoxia-selective retention have been proposed, both of which involve metal-centred one-electron reduction to give a copper(I) species. The first mechanism reported by Fujibayashi et al.[25] and Obata et al.[38] suggests that **1** is reduced enzymatically and trapped only within hypoxic tumour cells. The second mechanism proposed by Dearling et al.[36,37] is based on in vitro cellular accumulation and washout studies. Their results suggest that cellular uptake and intracellular reduction of **1** may occur within both normoxic and hypoxic tissue to give an unstable copper(I) species. This copper(I) species then becomes trapped intracellularly by virtue of its negative charge, which prevents cell washout by diffusion through the lipophilic cell membrane. The reversibility of cellular uptake and trapping is dependent on both the oxygen concentration and the relative stability of the copper(I) species, which may undergo rapid protonation, acid-catalysed dissociation, dimerisation or oxidation.

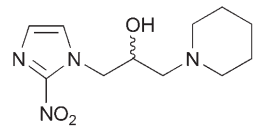
pimonidazole

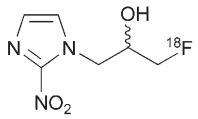
[^{18}F]-FMISO

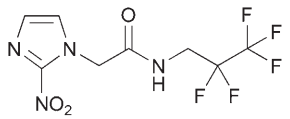
EF-5

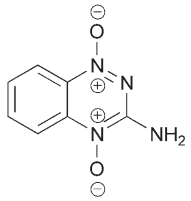
Tirapazamine (TZP)

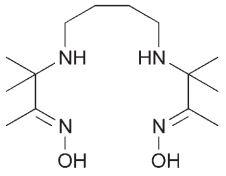
HL91

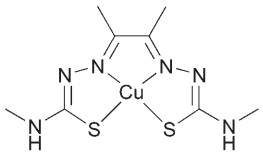
[Cu(II)ATSM]

The work presented in this article describes extensive electrochemical, spectroscopic and computational studies on the one-electron reduction and oxidation processes for a range of copper(II)–bis(thiosemicarbazonato) complexes. Cyclic voltammetry, combined with deconvolution analysis and digital simulations have been used to study the redox chemistry of these complexes. Electronic absorption (UV/Vis) and EPR spectroelectrochemistry (SEC) experiments have been conducted to provide further information on the nature of the reduced copper(I) species. Density functional

theory (DFT) and time-dependent density functional theory (TD-DFT) calculations have been performed to probe the electronic structure of the species involved and to understand the origins of the electronic transitions observed in the electronic absorption spectra. In addition, the X-ray crystal structures of three complexes are reported and the effect of acid on the electrochemistry and SEC for each copper(II) complex has been investigated. In combination with previously reported experimental and computational studies,[25,36–40] the results presented herein provide strong experimental support for the revised mechanism of hypoxia selectivity of copper(II)–bis(thiosemicarbazonato) complexes.

Results and Discussion

Synthesis and X-ray crystal structures: Structures of the copper(II) complexes described are shown in Scheme 1.[41] Complexes **1**–**6** and their corresponding proligands were synthesised in high yields in accordance with previously reported procedures.[42–45] X-ray crystal structures for **1** to **6** have also been reported.[46] All complexes have been characterised by elemental analysis, high-resolution mass spectrometry, reverse-phase gradient HPLC, UV/Vis spectroscopy, X-band EPR spectroscopy, cyclic voltammetry and DFT calculations.[40]

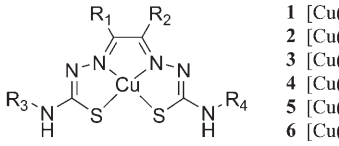

		R_1	R_2	R_3	R_4
1	[Cu(II)ATSM]	Me	Me	Me	Me
2	[Cu(II)PTSM]	Me	H	Me	Me
3	[Cu(II)PTS]	Me	H	H	H
4	[Cu(II)GTS]	H	H	H	H
5	[Cu(II)PTSE]	Me	H	Et	Et
6	[Cu(II)DTSM]	Et	Et	Me	Me

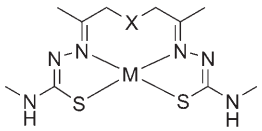

7 [Cu(II)L^1] X = S
8 [Cu(II)L^2] X = CH_2
9 [Zn(II)L^1] X = S

Scheme 1. Structures of the copper(II)–bis(thiosemicarbazonato) complexes investigated. For complexes **1**–**6**, the R_1 and R_2 groups are colloquially referred to as the backbone substituents and the R_3 and R_4 groups are bonded to the terminal nitrogen atoms. ATSM = diacetyl bis(4-*N*-methyl-3-thiosemicarbazonato)copper(II), PTSM = pyruvaldehyde bis(4-*N*-methyl-3-thiosemicarbazonato)copper(II), PTS = pyruvaldehyde bis(3-thiosemicarbazonato)copper(II), GTS = glyoxyl bis(3-thiosemicarbazonato)copper(II), PTSE = pyruvaldehyde bis(4-*N*-ethyl-3-thiosemicarbazonato)copper(II), DTSM = hexane-3,4-dione bis(4-*N*-methyl-3-thiosemicarbazonato)copper(II).

Complexes **7**–**9** were prepared in accordance with the procedures described by Gannon et al.[47] and the X-ray crystal structure of complex **7** is shown in Figure 1. Crystallographic data for all of the structures solved are given in Table 1 and selected experimental and DFT calculated geometric parameters for complexes **7**–**9** are given in Table 2.

Interestingly, black copper(II) complexes **7** and **8** and colourless zinc(II) complex **9**, exist as stereoisomers with the metal atom and the central sulfur atom (S3 in complexes **7** and **9**) or carbon atom (C11 in complex **8**) of the ligand backbone lying in the chiral C_2-axis of rotation (see the Supporting Information).[49] Complexes **1**–**6** have a square-planar copper(II) coordination geometry, whereas the metal

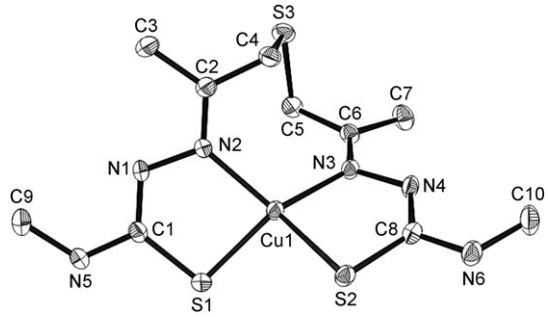

Figure 1. ORTEP[48] representation of the X-ray crystal structures of **7**. Thermal ellipsoids are shown at 50% probability and geometrically positioned hydrogen atoms have been omitted for clarity. The X-ray structures of complexes **8** and **9** are very similar and are presented in the Supporting Information.

Table 1. Crystallographic data for the copper(II) complexes **7** and **8** and zinc(II) complex **9** (CCDC structures 682479–682481).

	7	**8**	**9**
formula	$C_{10}H_{18}N_6S_3Cu$	$C_{11}H_{20}N_6S_2Cu$	$C_{10}H_{18}N_6S_3Zn$
M_r	382.04	366.01	383.87
T [K]	150	150	180
λ [Å]	0.71073	0.71073	0.71073
crystal system	orthorhombic	monoclinic	triclinic
space group	$P2_12_12_1$	$C2/c$	$\bar{P}1$
a [Å]	9.20520(10)	11.4427(2)	7.6720(2)
b [Å]	9.88260(10)	12.6442(3)	7.8933(2)
c [Å]	17.3326(2)	11.9986(2)	13.6261(4)
α [°]	90	90	83.0669(13)
β [°]	90	112.0859(12)	83.0139(13)
γ [°]	90	90	74.4332(12)
V [Å^3]	1576.77(3)	1608.62(6)	785.64(4)
Z	4	4	2
ρ_{calcd} [g cm^{-3}]	1.609	1.503	1.623
μ [mm^{-1}]	1.781	1.616	1.960
F(000)	788	756	396
size [mm]	0.08×0.20×0.30	0.08×0.09×0.19	0.05×0.20×0.50
crystal description	black plate	black plate	colourless plate
θ range [°]	$5.0 \le \theta \le 27.0$	$5.0 \le \theta \le 27.0$	$5.0 \le \theta \le 27$
index ranges	$-11 \le h \le 11$	$-14 \le h \le 13$	$-9 \le h \le 9$
	$0 \le k \le 12$	$0 \le k \le 16$	$0 \le k \le 10$
	$0 \le l \le 22$	$0 \le l \le 15$	$0 \le l \le 17$
reflns measured	22010	7889	12055
reflns unique	3566	1827	3513
R_{int}	0.035	0.030	0.048
reflns obsd ($I > 2\sigma(I)$)	3332	1449	4761
transmission coefficients (min/max)	0.78/0.87	0.82/0.88	0.67/0.91
parameters refined	182	94	181
R or $R1$ (obsd reflns)	$R = 0.0237$	$R = 0.0316$	$R = 0.0362$
wR or $R2$ (all data)	$wR = 0.0481$	$wR = 0.0766$	$wR = 0.0769$
GOF	0.953	0.9068	0.901
residual electron (min/max) [eÅ^3]	−0.63/0.36	−0.81/0.33	−0.59/0.48

Table 2. Selected experimental (X-ray) and calculated (DFT) geometric parameters for complexes **7–9**. X-ray crystal structure values with estimated standard deviations (esd values) are presented first followed by the calculated values from DFT geometry optimisations.[a]

	7		**8**		**9**	
	exptl (esd)	calcd	exptl (esd)	calcd	exptl (esd)	calcd
r(C1–N1)	1.302(3)	1.316	1.304(3)	1.314	1.319(3)	1.321
r(N1–N2)	1.404(2)	1.377	1.402(3)	1.380	1.395(3)	1.374
r(N2–C2)	1.297(3)	1.303	1.292(3)	1.300	1.287(3)	1.300
r(C1–N5)[b]	1.357(3)	1.359	1.356(3)	1.360	1.345(3)	1.358
r(C1–S1)	1.751(2)	1.761	1.754(3)	1.761	1.756(2)	1.768
r(M–S1)	2.2399(6)	2.269	2.2223(7)[c]	2.273	2.2721(7)	2.316
r(M–S2)	2.2202(6)	2.269	2.2223(7)[c]	2.273	2.3162(7)	2.316
r(M–N2)	2.0192(18)	2.089	2.030(2)[c]	2.090	2.054(2)	2.106
r(M–N3)	2.0270(18)	2.089	2.030(2)[c]	2.090	2.028(2)	2.106
r(M···S3)	4.148	4.234	–	–	4.089	4.209
r(M···C11)	–	–	3.878	3.941	–	–
a(C1-N1-N2)	113.94(18)	115.2	113.8(2)	115.1	113.41(19)	115.3
a(S1-C1-N1)	126.10(17)	126.7	126.0(2)	126.7	127.71(19)	127.9
a(M-S1-C1)	94.82(7)	94.8	95.24(9)	94.9	90.64(9)	91.6
a(N2-M-S1)	85.95(5)	85.4	144.14(6)[c]	85.3	85.90(6)	85.3
a(N2-M-N3)	110.63(8)	111.5	112.60(12)	111.6	117.35(8)	113.5
a(N3-M-S2)	86.01(6)	85.4	144.14(6)[c]	85.3	84.82(6)	85.3
a(S1-M-S2)	94.81(2)	96.5	96.06(5)	95.5	127.19(3)	124.0
RMSD[d]	0.168		0.122		0.222	

[a] Bond lengths and distances are given in Å, and bond angles in degrees [°]. M refers to either Cu1 in complexes **7** and **8** or Zn1 in complex **9**. [b] Equivalent to *r*(C1-N3)/Å for complex **8**. [c] Related by two-fold rotation. [d] Root-mean-square deviation (RMSD) in Å, calculated using all non-hydrogen atoms between the X-ray crystal structure and the DFT optimised gas phase geometry.

ions in complexes **7–9** have a distorted pseudo-tetrahedral structure with dihedral angles defined by the two planes of the thiosemicarbazonato groups of 49.5 and 49.0°, respectively. The distorted tetrahedral geometry of **7** and **8** is a result of the steric requirements of the longer 1,5-bis(thiosemicarbazonato) ligands (L^1 and L^2). This change in geometry has important consequences on the electronic structures of **7** and **8**, which is evident in the electrochemistry and UV/Vis and EPR spectroscopies (see below).

The X-ray crystal structure of the Δ enantiomer of zinc(II) complex **9** is more highly distorted towards tetrahedral geometry than the analogous copper(II) complex **7**. The dihedral angle defined by best planes of the two thiosemicarbazonato groups opens to −105.3°. Most zinc(II)–bis(thiosemicarbazonato) complexes, such as the zinc(II) analogue of complex **1**, [Zn(II)ATSM], are bright yellow in solution and weakly fluorescent with an electronic absorption band at around 430 nm, and peak emissions between 520 and 580 nm.[41] This emission has allowed cellular uptake and intracellular localisation to be investigated by confocal and epifluorescent microscopy.[41,50] In contrast, complex **9** is colourless and non-fluorescent. The different electronic absorption and emission properties of **9** are a result of the steric requirements of the ligand and the preferred tetrahedral coordination geometry of the zinc(II) ion, which causes a loss of pπ-orbital conjugation.

DFT optimised geometries of complexes **1–9** are in excellent agreement with the experimentally determined structures (Table 2).[46] Weighted root-mean-square deviations (RMSD) calculated for all non-hydrogen atoms, between the X-ray crystal structures and the DFT optimised gas-phase geometries are typically <0.22 Å.

Electrochemistry: The electrochemistry of copper(II)–bis(thiosemicarbazonato) complexes **1–6**, has been reported previously.[36,37] However, the most detailed of these studies only compared the half-wave potentials ($E_{1/2}$) for the reduction and oxidation of the copper(II) species in anhydrous, deoxygenated DMSO.[36,37] The effect of water, pH and dissolved oxygen (all crucial components of the intracellular environment) on the electrochemistry have not been investigated. Consequently, the lack of detailed knowledge on the nature and fate of the reduced copper(I) species has lead to rather speculative proposals on the mechanism of hypoxia selectivity for complexes such as **1**.[25,36–39]

Experimental parameters derived from the cyclic voltammograms (CVs) of copper(II) complexes **1–8** are presented in Table 3. Half-wave potentials ($E_{1/2}$(SCE)) peak separation (ΔE_p) and the ratio of peak currents ($|i_{pa}|/|i_{pc}|$) for one-electron reduction and oxidation processes are given. All potentials are reported relative to the saturated calomel reference electrode (SCE) and have been corrected by using the one-electron oxidation of ferrocene (Fc/Fc^+) as an internal reference. The full potential sweep width CV (current versus potential curve) of a 5.0×10^{-3} mol dm^{-3} solution of complex **1**, for three complete cycles at 100 mV s^{-1}, is shown in Figure 2a. CVs have also been analysed by convolution potential sweep voltammetry (CPSV)[51] and the semi-integral[52] (Figure 2b) and semi-derivative[53,54] (Figure 2c) of the experimental current versus potential curve for **1** are also shown.

Figure 2a is representative of the CVs observed for all of the copper(II)–bis(thiosemicarbazonato) complexes studied. Complex **1** exhibits two quasi-reversible redox processes labelled A/B and C/D, with $E_{1/2}$ values of +0.734 and −0.646 V, respectively. The quasi-reversibility of redox couples A/B and C/D is most evident in the peak shapes of the semi-integral shown in Figure 2b. Stirred voltammetry experiments confirmed that redox couples A/B and C/D correspond to the oxidation and reduction processes, respectively. The E/F redox couple is discussed in the Acid Titrations section below. Extensive SAR studies found that hypoxia selectivity strongly correlates with both the half-wave potential

Table 3. Cyclic voltammetry data for reduction of copper(II)–bis(thiosemicarbazonato) complexes recorded under a nitrogen atmosphere at 295 K, in anhydrous, deoxygenated DMF at 100 mV s^{-1} with a platinum macrodisc working electrode.

	Cu^{II}/Cu^{I} Reduction[a]									Oxidation[b]		
	ΔE_p [V][c]	$\lvert i_{pa}\rvert/\lvert i_{pc}\rvert$[d]	$E_{1/2}$ (SCE) [V][e]	D_O [$\times 10^{-6}$ cm^{2}s^{-1}]	D_R [$\times 10^{-6}$ cm^{2}s^{-1}]	n_a	n_c	W_{pa} [V]	W_{pc} [V]	ΔE_p [V][c]	$\lvert i_{pc}\rvert/\lvert i_{pa}\rvert$[d]	$E_{1/2}$ (SCE) [V][e]
1	0.095	0.989	−0.646	2.324	2.500	0.869	0.807	0.106	0.118	0.075	0.945	0.734
2	0.098	0.852	−0.565	2.929	2.854	0.974	0.785	0.103	0.131	0.078	0.497	0.765
3	0.088	0.880	−0.557	2.436	1.825	0.825	0.911	0.112	0.119	0.070	0.870	0.755
4	0.110	0.927	−0.458	3.814	3.634	0.871	0.933	0.118	0.117	0.074	0.650	0.782
5	0.148	0.683	−0.580	1.809	2.020	0.727	0.894	0.123	0.135	0.084	0.378	0.749
6	0.085	0.774	−0.637	1.746	1.584	0.958	0.932	0.109	0.111	0.065	0.813	0.717
7	0.107	1.033	−0.338	3.036	2.296	0.890	0.801	0.101	0.096	0.114	0.392	0.789
8	0.071	0.935	−0.430	4.771	4.487	0.862	0.818	0.098	0.095	0.116	0.418	0.751

[a] Corresponding to the redox couple labelled C/D in Figure 2a and c. All potentials are quoted relative to SCE. [b] Redox couple A/B. [c] The difference in peak potentials is given by $\Delta E_p = E_{pa} - E_{pc}$. [d] Ratio of peak currents at 100 mV s^{-1} for the one-electron reduction couple, C/D. [e] The half-wave potential is given by $E_{1/2} = (E_{pa} + E_{pc})/2$. The *n*-values are derived from the peak-to-half-peak $|E_p - E_{p/2}|$ separations in the CVs (see the Supporting Information).

of the reduction process and the alkyl substitution pattern on the ligand backbone.[37]

Figure 3 shows the scan-rate dependence of the CV for the one-electron reduction of complex **1** and the plot of peak currents (i_p) versus the square root of the scan rate ($\upsilon^{1/2}$). The Randles–Sevcik equation has been used to calculate the diffusion coefficients (D) of the copper(II) and the corresponding reduced copper(I) species (Table 3).[55] The effective electrochemically active area ($A = 0.02$ cm^2) of the working electrodes was calculated from the reversible one-electron oxidation of 5.0×10^{-3} mol dm^{-3} ferrocene ($D_{Fc/Fc+} = 1.07 \times 10^{-5}$ cm^2 s^{-1})[56] in anhydrous, deoxygenated DMF. For the C/D reduction couple, the peak separation at 100 mV s^{-1} of $\Delta E_p = 95$ mV, and the peak current ratio ($|i_{pa}|/|i_{pc}|$) of 0.989 along with the calculated *n* values < 1.0 are indicative of a quasi-reversible electron-transfer process. In comparison, the A/B oxidation couple is more reversible at 295 K, with $\Delta E_p = 75$ mV, and $|i_{pc}|/|i_{pa}| = 0.945$. At both platinum and gold macrodisc electrodes, the peak separation increases linearly with the square root of the scan rate (Figure 3b). On successive cyclic voltammetry cycles performed within the same experiment, the peak separation of the A/B couple remains constant. However, for the C/D couple, the peaks diverge slightly and both the cathodic and anodic peak currents decrease equally, which indicates a possible decrease in concentration of the redox-active species present.

Deconvolution analysis of the CV of **1** further supports the quasi-reversible assignment for the C/D reduction couple (Figure 2c). The semi-derivative $E_{1/2}$ value of −0.645 V is in agreement with the value derived from the normal CV and the cathodic and anodic half-peak widths were found to be $W_{pc} = 118$ mV and $W_{pa} = 106$ mV, respectively. The number of electrons transferred in the cathodic and anodic sweeps were calculated to be $n_c = 0.760$ and $n_a = 0.846$ electrons, respectively, by plotting the semi-derivative peak potentials (e_p versus scan rate (υ)) and by using the experimental diffusion coefficients ($n_c = 0.884$ and $n_a = 0.798$ electrons).[53,54]

DigiSim3.03[57] was used to perform digital simulations of the CVs for the one-electron reduction of **1** at the gold macrodisc working electrode. The same electrochemical behaviour was observed with both the platinum and gold macrodisc working electrodes. The experimental and simulated CVs at 250 mV s^{-1} are shown in Figure 3c and further details are given in the Supporting Information. The electron-transfer process was modelled by using Equation (1):

$$O + e^- \overset{k_s,\alpha}{\rightleftharpoons} R \quad (1)$$

Simulations were used to determine the transfer coefficient (α), which is a measure of the symmetry of the energy barrier to electron transfer, the heterogeneous rate constant (k_s) and the diffusion coefficients of the oxidised (D_O) and reduced species (D_R) with varying scan rates. At 100 mV s^{-1}, α is 0.58 ± 0.07, which indicates that the transition state for electron transfer lies slightly closer to the geometry of the copper(II) species than the reduced copper(I) species.[55] The heterogeneous rate constant (k_s) is (0.0125 ± 0.0017) cm s^{-1}, which is of the correct order of magnitude for a quasi-reversible electron-transfer process. The simulated anodic current is slightly larger than the experimental value and potential origins of this feature are discussed below. The simulated diffusion coefficients (D_O) for **1** is $(4.91 \pm 0.07) \times 10^{-6}$ cm^2 s^{-1} and for the reduced copper(I) species $D_R = (6.77 \pm 0.45) \times 10^{-6}$ cm^2 s^{-1}; these values compare favourably with the experimental values of $D_O = 2.324 \times 10^{-6}$ cm^2 s^{-1} and $D_R = 2.500 \times 10^{-6}$ cm^2 s^{-1} (Table 3). The experimental and simulated diffusion coefficients are of the correct order of magnitude. However, the absolute experimental values are subject to errors derived from the use of the Randles–Sevcik equation, which assumes that $n = 1.0$ and that the redox process is electrochemically reversible.

DFT calculations: Recent DFT calculations of solution-phase one-electron reduction potentials and absolute pK_a values for complexes **1**–**4** showed that reduction is metal-centred, leading to the formation of closed-shell copper(I) species with d^{10} electron configurations.[40] Ligand-based reduction to form a reduced triplet species was found to be 57.0 kJ mol^{-1} less stable than the formation of the copper(I) singlet for **1**. Figure 4 shows the spatial distributions of the

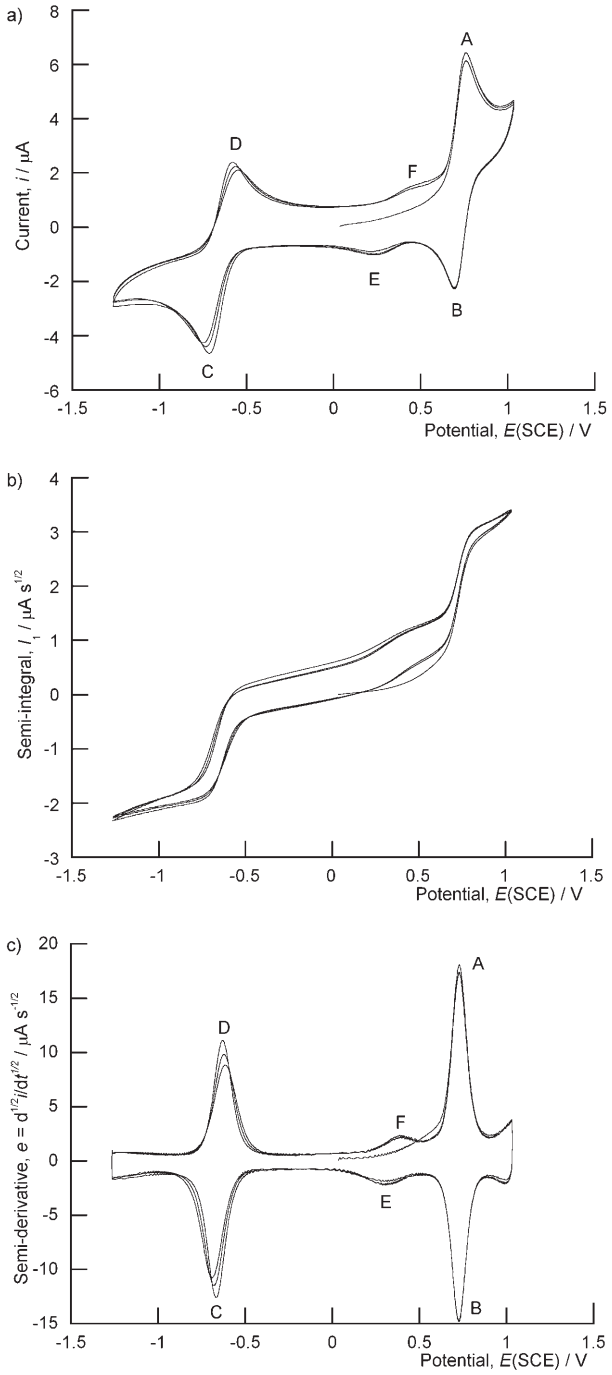

Figure 2. a) Full potential sweep width CV of a 5.0×10^{-3} mol dm^{-3} solution of **1** recorded by using a platinum disc working electrode at 100 mV s^{-1} in anhydrous, deoxygenated DMF at 295 K. Three complete cycles were recorded starting with positive sweep polarity at +0.036 V, and switching directions at +1.035 V and −1.266 V. Convolution analysis has been used to plot b) the semi-integral (I_1 [μA s$^{1/2}$]) and c) the semi-derivative ($e = d^{1/2}i/dt^{1/2}$ [μA s$^{-1/2}$]) of the cyclic voltammetry data. Redox processes A–F in Figure 2a and c are discussed in the main text.

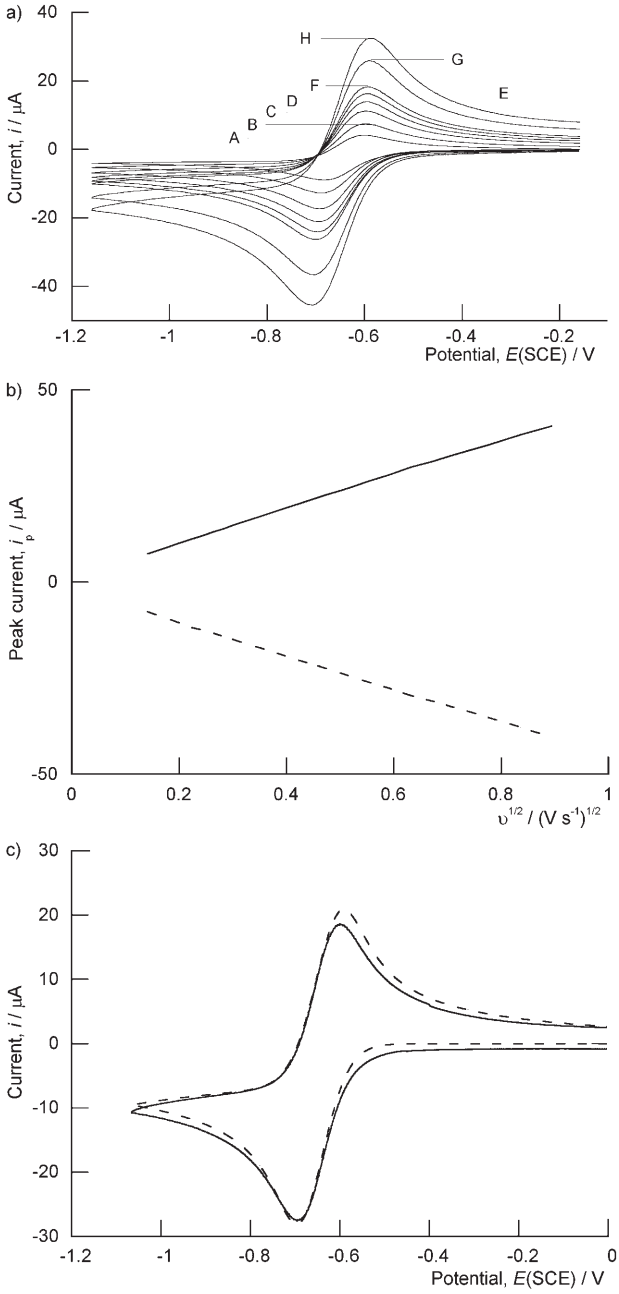

Figure 3. a) Scan-rate dependence of the CVs for the one-electron reduction of a 5.0×10^{-3} mol dm^{-3} solution of **1** in anhydrous, deoxygenated DMF at 295 K by using the platinum macrodisc working electrode. Scan rate: 20 (A), 50 (B), 100 (C), 150 (D), 200 (E), 250 (F), 500 (G) and 800 mV s^{-1} (H). b) Plot of cathodic (-----) and anodic (——) peak currents versus the square root of the scan rate. c) Experimental (——) and digital simulation (-----) of the one-electron reduction of **1** at 250 mV s^{-1}. $\alpha = 0.58\pm0.05$, $k_s = (0.0148\pm0.0015)$ cm s^{-1}, $D_O = (4.92\pm0.06)\times10^{-6}$ cm^2 s^{-1} and $D_R = (6.68\pm0.41)\times10^{-6}$ cm^2 s^{-1}.

lowest unoccupied molecular orbital (βLUMO) for the neutral copper(II) species that accepts the electron on reduction and becomes the highest occupied molecular orbital (βHOMO) in the copper(I) anion. The coordination geometry changes from square-planar in the neutral copper(II) species to pseudo-tetrahedral in the reduced copper(I) anion. This structural twist is accompanied by a change in the dihedral angle (d(N=C−C=N)) of the diimine backbone, which opens from 0.0° in all copper(II)–bis(thiosemicarbazonato) complexes to −26.4 and −22.5° in DFT optimised

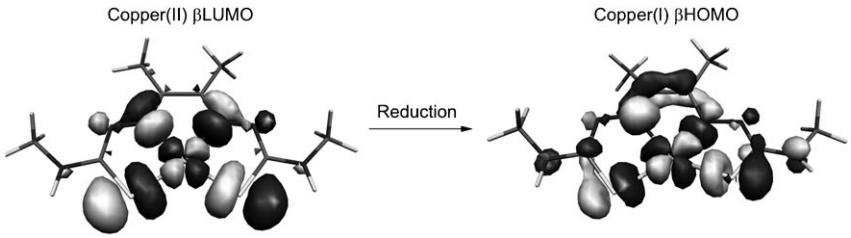

Figure 4. MO isosurfaces showing the spatial distribution of the neutral **1** βLUMO and the anionic $[Cu^{I}ATSM]^{-}$ βHOMO. On reduction, the coordination geometry changes from square-planar to pseudo-tetrahedral.

structures of copper(I) anions of complexes **1** and **2**, respectively.

The predicted change to a pseudo-tetrahedral coordination geometry on reduction to the copper(I) species is consistent with the quasi-reversible behaviour observed in the electrochemistry and the simulated value of the transfer coefficient (α). DFT calculations are also consistent with experimental results on the only copper(I)–bis(thiosemicarbazonato) species to have been isolated and characterised by X-ray crystallography, the novel dicationic copper(I) helical dimer **1d**.[58] Each copper(I) ion has a tetrahedral coordination mode in which one nitrogen and one sulfur donor atom is provided from each of the bis(thiosemicarbazone) ligands. The optimised geometry of **1d** (Figure 5) is in excellent

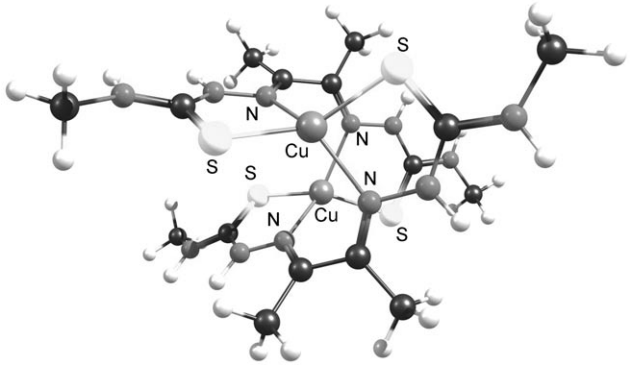

Figure 5. DFT optimised geometry of the copper(I) helical dimer **1d**[58] obtained by using uB3LYP/6-31++G(d,p) methodology (C_1 symmetry using 914 basis functions). The optimised geometry has pseudo-D_2 symmetry. X-ray(esd)/DFT: r(Cu1–N1) = 2.112(2)/2.198 Å, r(Cu1–N3) = 2.111(2)/2.198 Å, r(Cu1–S1) = 2.2658(9)/2.318 Å, r(Cu1–S2) = 2.2729(9)/2.318 Å, r(Cu1···Cu2) = 3.562/3.494 Å, d(N1=C1–C2=N2) = 51.2/50.5° (see the Supporting Information).

agreement with the X-ray crystal structure, with a weighted RMSD calculated for all 34 non-hydrogen atoms of only 0.502 Å. Isolation of this dimeric species suggests that intracellular reduction to the copper(I) species is likely to be complicated by protic equilibria, ligand dissociation and potential dimerisation (see below).

The one-electron A/B oxidation couple of **1** and other copper(II)–bis(thiosemicarbazonato) complexes has previously been assigned to the Cu^{III}/Cu^{II} redox process.[37] However, the nature of the oxidation is uncertain and it is possible that the electron is removed from an orbital based on either the copper(II) ion or the ligand to give a cationic singlet or triplet species, respectively. DFT calculations indicate that for complexes **1**–**4**, ligand-based oxidation to give the cationic triplet species is thermodynamically favoured over the formation of the copper(III) ion.

In the gas phase the difference in calculated free energies for electron attachment, $\Delta\Delta_{EA}G^0$ (triplet–singlet) for the oxidised cationic species $\mathbf{1}^+$–$\mathbf{4}^+$ were found to be −12.8, −17.0, −23.4 and −25.4 kJ mol^{-1}, respectively. This energy difference decreases as electron-donating methyl substituents are placed on either the ligand backbone (R_1 and R_2) or terminal nitrogen positions (R_3 and R_4). In both the singlet-$\mathbf{1}^+$ and triplet-$\mathbf{1}^+$ species, the coordination geometry of the copper ion remains square-planar on oxidation. However, in the singlet-$\mathbf{1}^+$ species, the metal–ligand bond lengths, r(Cu–S) and r(Cu–N), decrease by around 0.100 Å, whereas in the triplet-$\mathbf{1}^+$ species they remain within 0.010 Å of the calculated structure of **1**. Formation of the triplet-$\mathbf{1}^+$ species involves the removal of the electron from the copper(II) βHOMO, which has ligand-based ππ* character. In contrast, formation of the singlet-$\mathbf{1}^+$ species involves removal of the electron from the copper(II) αHOMO-1, metal-based, σ* antibonding orbital, which causes the decrease observed in the calculated metal–ligand bond lengths. Figure 6 shows the schematic MO diagram of the triplet-$\mathbf{1}^+$ species. Further MO diagrams and DFT calculated redox potentials for complexes **1**–**8** are presented in the Supporting Information.

An excellent correlation was found between the difference in one-electron oxidation and reduction half-wave potentials ($E_{A/B}$(ox)−$E_{C/D}$(red)) versus the wavenumber of the lowest-energy electronic absorption band ($\tilde{\nu}$) for copper(II) complexes **1**–**8** (R value = 0.984). This indicates that the nature of redox couples A/B and C/D is the same for each copper(II) complex (see the Supporting Information).

Although oxidation of copper(II)–bis(thiosemicarbazonato) complexes is not thought to be involved in the mechanism of hypoxia selectivity, complex **1** and other related lipophilic complexes are known to accumulate in the liver, where, for example, oxidation by P450 enzymes may provide an important biochemical pathway for excretion.

UV/Vis SEC in deoxygenated DMF: The structure and chemical stability of the copper(I) species formed on reduction of copper(II)–bis(thiosemicarbazonato) complexes in anhydrous DMF have been investigated by in situ UV/Vis and EPR SEC. For the UV/Vis SEC measurements, changes in the electronic absorption spectra during both electro-

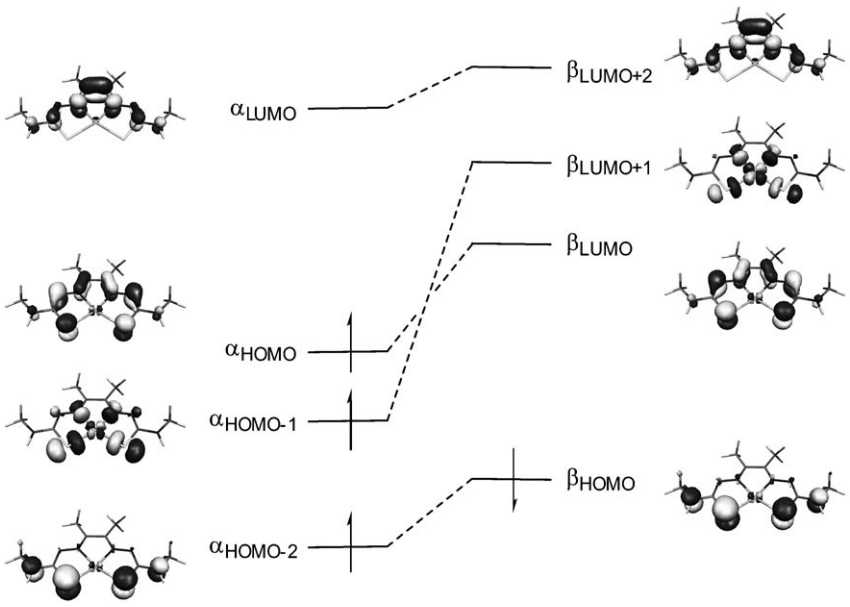

Figure 6. Schematic MO diagram of the oxidised cationic triplet-$\mathbf{1}^{+}$ species.

chemical reduction and oxidation of 1.0×10^{-3} mol dm^{-3} solutions of complexes **1**–**8** were monitored by using an optically transparent thin-layer electrochemical (OTTLE) cell (path length, $l=0.46$ mm).[59] Full details of the experimental conditions and apparatus used are given in the Experimental Section and the Supporting Information.

Figure 7a shows the changes observed in the electronic absorption spectrum between 800 and 270 nm during the electrochemical reduction of **1** at an applied potential (E_{appl}) of −0.959 V in anhydrous, deoxygenated DMF. The initial UV/Vis spectrum of **1** has been reported previously,[60] and more recently, we have used TD-DFT calculations to assign the experimental absorption bands.[41] Six well-defined isosbestic points are observed at 565, 410, 382, 347, 327 and 288 nm, which demonstrates that electrochemical reduction proceeds cleanly in deoxygenated DMF to give a single, reduced copper(I) species. The solution changes colour from red to yellow as the peak absorbance at 478 nm ($\varepsilon=$ 7855 mol^{-1} dm^3 cm^{-1}) decreases during electrochemical reduction. Two new weaker absorption bands appear at longer wavelengths with peaks at 497 nm ($\varepsilon=1347$ mol^{-1} dm^3 cm^{-1}) and 606 nm ($\varepsilon=1164$ mol^{-1} dm^3 cm^{-1}) and a shallow minimum at 565 nm ($\varepsilon=1055$ mol^{-1} dm^3 cm^{-1}). The absorbance increases in the region between 775 and 565 nm. At shorter wavelengths, both the intense peak and shoulder at 314 and 355 nm, associated with metal-to-ligand charge-transfer and ligand-based π–π* transitions, undergo a slight redshift and a decrease in absorption intensity on reduction to 328 nm ($\varepsilon=19460$ mol^{-1} dm^3 cm^{-1}) and 382 nm ($\varepsilon=$ 6340 mol^{-1} dm^3 cm^{-1}), respectively.

Figure 7b shows the change in the UV/Vis spectrum of the reduced copper(I) species of **1** after electrochemical reduction. Again, six well-defined isosbestic points are observed at the same wavelengths as those for the reduction step and after 25–30 min, the spectrum is indistinguishable from that of the initial spectrum of **1**. The UV/Vis spectrum of the reduced copper(I) species of **1** is similar to that of the pseudo-tetrahedral copper(II) complex **7** (see the Supporting Information). This data provides the first spectroscopic evidence in support of the DFT calculations that predict a change from square-planar to pseudo-tetrahedral coordination geometry on reduction of complexes **1**–**6**.[40]

Figure 8 shows the change in peak absorbance at 478 nm during four successive electrochemical reduction and reoxidation cycles of **1**. In deoxygenated DMF, the peak absorbance decreased immediately at the start of the experiment (Figure 8 point A). After approximately 6.0 min, all of **1** within the optical window was quantitatively reduced to give a stable, pale yellow copper(I) species.[39] The potentiostat was then switched to open circuit (no potential) and an immediate increase in absorbance was observed due to rapid oxidation of the copper(I) species by residual molecular oxygen, O_2(sol), diffusing into the OTTLE cell (Figure 8 point B). After 40 min, the peak absorbance at 478 nm recovered to 99.5 % of the initial value. At points C, E and F, three further bulk electrochemical reduction cycles were performed at applied potentials of −0.859, −0.759 and −0.709 V. Rapid electrochemical oxidation of the reduced copper(I) species was achieved by using an applied potential of +0.041 V (Figure 8point D). This experiment demonstrates that electrochemical reduction of **1** is fully reversible on a bulk scale and in the absence of acid or water gives a single, reduced copper(I) species, which is stable with respect to ligand dissociation. Further evidence of the bulk scale reversibility was provided by performing in situ UV/Vis spectrovoltammetry (see the Supporting Information).

For complexes **1**–**8** Nernstian plots of the applied potential (E_{appl}(SCE)) versus log([O]/[R]) for the one-electron reduction in anhydrous, deoxygenated DMF show a linear relationship. For example, for complex **2**, the standard reduction potential is $E^{o'}$ (SCE) = −0.566 V and the number of electrons transferred is $n=1.02$, which are in excellent agreement with the values determined from cyclic voltammetry (Table 3 and the Supporting Information).[59]

For the first time, the electronic structure of the reduced copper(I) species has been characterised by electronic absorption spectroscopy and it has been demonstrated that oxygen is capable of oxidising this species. Further experiments showed that diffusion of **1** from the bulk solution into

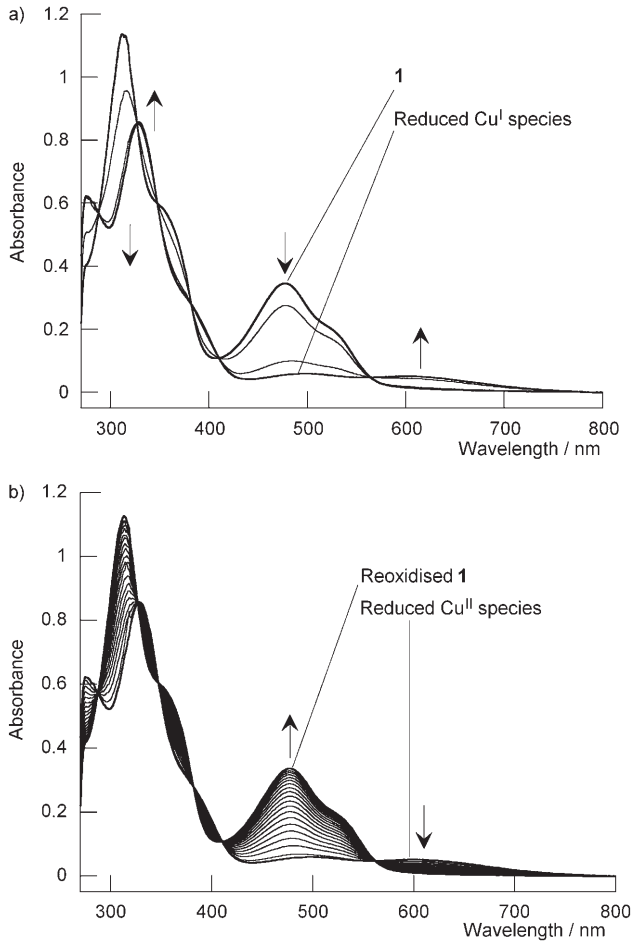

Figure 7. a) Change in the experimental UV/Vis absorption spectrum of a 1.0×10^{-3} mol dm^{-3} solution of **1** in anhydrous, deoxygenated DMF measured during electrochemical reduction at E_{appl}(SCE) = −0.959 V. Bulk electrolysis was performed for 321 s until the final current was 6.00% of the initial current passed at $t=0$ s. The arrows indicate the direction of change in absorbance from the initial complex (**1**) to the reduced copper(I) species formed. b) Change observed in the UV/Vis spectrum after electrochemical reduction at open circuit. After 25 min the peak absorbance at 478 nm returned to 97.6% of the initial absorbance of **1**. Experimental difference spectra are given in the Supporting Information. Approximately 1.5×10^{-7} mol of solute is reduced at the working electrode during the UV/Vis SEC experiments.

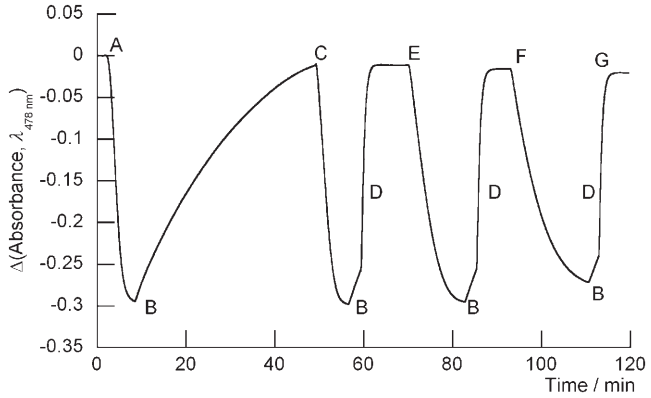

Figure 8. Time-resolved change observed in the experimental UV/Vis peak absorbance at 478 nm of a 1.0×10^{-3} mol dm^{-3} solution of **1** in anhydrous, deoxygenated DMF on successive electrochemical reduction and reoxidation cycles. A) Electrochemical reduction at −0.959 V for 376 s to $i=5.40$% of the initial current. B) Immediate increase in absorbance between 510 and 2950 s due to reoxidation by residual molecular oxygen, O_2(sol). The later points include a small contribution from diffusion of **1** from the bulk solution. C) The peak absorbance returned to 99.5% of the initial value. Reduction at −0.859 V for 437 s to $i=6.25$%. D) Rapid electrochemical reoxidation at +0.041 V for 230 s to $i=2.00$%. E) Reduction at −0.759 V for 757 s to $i=7.00$%. F) Reduction at −0.709 V for 1050 s to $i=7.69$%. G) Final absorbance change of −0.0206 at 7200 s, which represents an overall recovery of 97.9% of the peak absorbance at 478 nm after 2 h, and four redox cycles.

the optical window is much slower than the observed rate of oxidation of the copper(I) species by dioxygen (see below and the Supporting Information). Even though the solutions were deoxygenated by a vigorous nitrogen purge and the apparatus was sealed with a Teflon lid, a small amount of dioxygen, which is highly soluble in DMF, is likely to remain present in solution. Reduction of dioxygen in aprotic, anhydrous solvents has been described previously.[61–64] In the absence of a source of protons, the superoxide radical anion is formed by the quasi-reversible one-electron reduction of dioxygen. Maricle and Hodgson report a half-wave potential of −0.80 V (versus SCE), recorded by using a dropping mercury electrode (DME),[61] whereas Vasudevan and Wendt report a half-wave potential of −0.780 V, with a cathodic peak potential of −0.855 V, using cyclic voltammetry with a glassy carbon electrode.[64]

In the present study, the onset of the cathodic wave for the one-electron reduction of dioxygen at the platinum macrodisc electrode was found to occur at approximately −0.48 V versus SCE. In the presence of a proton source (trace water or substrate), the mechanism of dioxygen reduction changes to a two-electron process, which occurs at the same potential as the formation of the superoxide radical anion. The dismutation reaction of superoxide with water or acid can lead to the formation of highly reactive oxygen species, such as $HO_2^{\bullet}$, H_2O_2, HO_2^- and HO^- [Eq. (2) and (3)].[61] The reactions of each of these reactive oxygen species with copper(II)–bis(thiosemicarbazonato) complexes have not been investigated.

$$2O_2^{\bullet-}+H_2O \rightarrow HO_2^-+O_2+HO^- \quad (2)$$

$$2HO_2^{\bullet} \rightarrow H_2O_2+O_2 \quad (3)$$

$$[Cu^{I}L]^-+O_2 \xrightarrow{\Delta_r G^\circ(sol)} [Cu^{II}L]+O_2^{\bullet-} \quad (4)$$

The energetics of the reaction between the reduced copper(I) anions of complexes **1**–**4**, **7** and **8**, and dioxygen to give the corresponding neutral copper(II) complex and superoxide [Eq. (4)] have been modelled by using DFT calculations. Calculations indicate that the spin-forbidden reaction between triplet ground state oxygen and the singlet reduced copper(I) species is highly endothermic in the gas phase. However, when solvation effects are incorporated by

using either a water or DMF polarisable continuum model, the reaction becomes spontaneous for all complexes with the exception of complexes **4** and **7**. Complexes with more negative Cu^{II}/Cu^{I} reduction potentials, and therefore, a more easily oxidised copper(I) anion, are predicted to react spontaneously with dioxygen. For example, complex **1** has a calculated reduction potential in DMF of −0.569 V, and a reaction free energy ($\Delta_r G^o$ (DMF)) of $-22.8\,kJ\,mol^{-1}$. Further details are presented in the Supporting Information.

UV/Vis SEC in aerated DMF: UV/Vis SEC reduction of the copper(II)–bis(thiosemicarbazonato) complexes were also performed in aerated DMF. Figure 9 shows the change

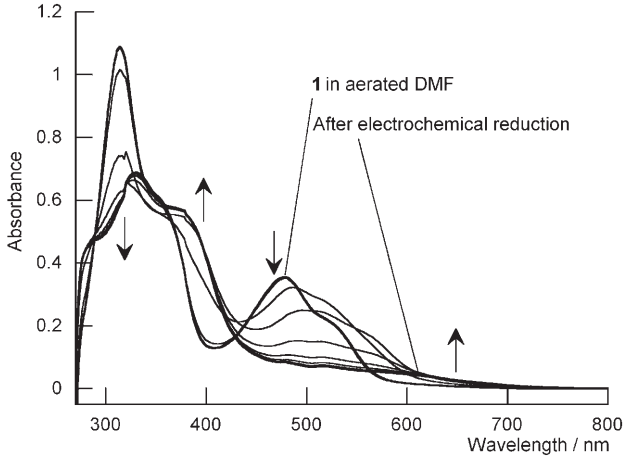

Figure 9. Change in the experimental UV/Vis spectrum of a $1.0\times10^{-3}\,mol\,dm^{-3}$ solution of **1** in anhydrous, aerated DMF during electrochemical reduction at $E_{appl}(SCE) = -0.959$ V. Bulk electrolysis was performed for 907 s until the final current was 19.70% of the initial current passed at $t = 0$ s. The arrows indicate the direction of change in absorbance from the initial complex (**1**) to the final spectrum recorded during reduction.

in the electronic absorption spectrum during electrochemical reduction of **1** in the presence of atmospheric dioxygen. In contrast with the results obtained in deoxygenated DMF (Figure 7), no isosbestic points were observed, which indicated that reduction in the presence of O_2(sol) is complicated by one or more solution-phase reactions that form intermediate chromophores. In the deoxygenated solution, the total charge transferred from the electrode to the solution was 15.2 mC. However, in the aerated solution 41.1 mC was transferred in the same period of time. The additional charge transferred is assigned to the initial in situ reduction of dioxygen and the formation of superoxide.

Figure 10 shows the change in peak absorbance at 478 nm versus time for the reduction of **1** in deoxygenated and aerated DMF, and the corresponding change observed during electrochemical oxidation (for 1200 s at +1.041 V) to form the triplet-$\mathbf{1}^+$ species in deoxygenated DMF. In contrast with the immediate and rapid decrease in peak absorbance observed for reduction in the absence of O_2(sol), in the aerated solution an induction period of approximately 45 s, in

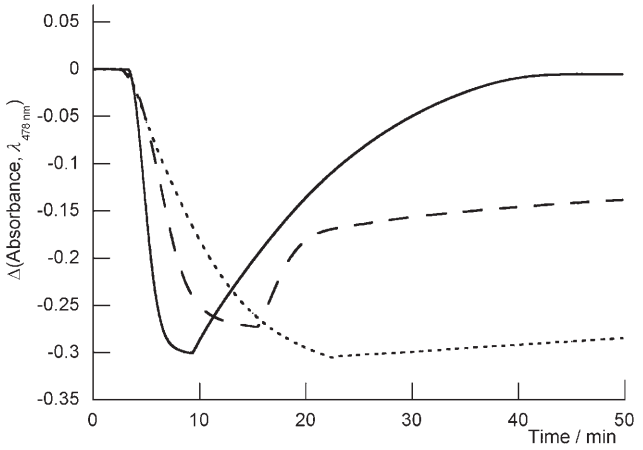

Figure 10. Change in the peak absorbance at 478 nm versus time for the one-electron reduction of **1** in deoxygenated (——) and aerated (– – –) DMF, and the one-electron electrochemical oxidation of **1** in deoxygenated DMF (-----).

which the absorbance decreased by less than 1.0%, was observed. This induction period corresponds to the facile reduction of dioxygen at the platinum mesh electrode. After 45 s, the absorbance begins to decrease more rapidly, but still at a slower rate than for reduction in deoxygenated solution. A smaller overall change in absorbance is observed in the presence of O_2(sol) due to the absorbance of other chromophores present in solution. Figure 10 also demonstrates that in aerated solution, oxidation of the reduced copper(I) species is more rapid than in deoxygenated DMF. Interestingly, in six separate aerated experiments, the final absorbance at 478 nm returned reproducibly to (61.1 ± 1.4)% of the initial absorbance. This difference is assigned to the solution-phase reaction of **1** with the electrogenerated superoxide. Copper(II)–bis(thiosemicarbazonato) complexes have been shown to possess superoxide dismutase-type reactivity.[65–67]

On the cyclic voltammetry timescale, one-electron oxidation (A/B couple) is found to be almost reversible (Figure 2). However, in the OTTLE cell in deoxygenated DMF, bulk electrochemical oxidation of **1** is irreversible. The absorbance at 478 nm is absent after electrochemical oxidation and when the potentiostat is switched to open circuit, the absorbance increases linearly due to slow diffusion of **1** from the bulk solution into the optical window. The rate of background diffusion is constant in all experiments, as shown by the equal gradients of the line for reduction under aerated conditions and electrochemical oxidation at times >25 min (Figure 10). This data provides further confirmation that dioxygen is able to rapidly oxidise the reduced copper(I) species.

TD-DFT calculations: The electronic absorption spectrum of **1** has been simulated and assigned by using TD-DFT calculations.[41] To understand the electronic structure of the reduced copper(I) species, TD-DFT calculations using Gaussi-

an 03 were performed on the optimised geometry of the copper(I) anionic complex, $[Cu^{I}ATSM]^{-}$.[68]

The simulated electronic absorption spectrum of $[Cu^{I}ATSM]^{-}$, is in excellent agreement with the experimental UV/Vis spectrum of the reduced copper(I) species (Figure 11 and the Supporting Information). The simulated

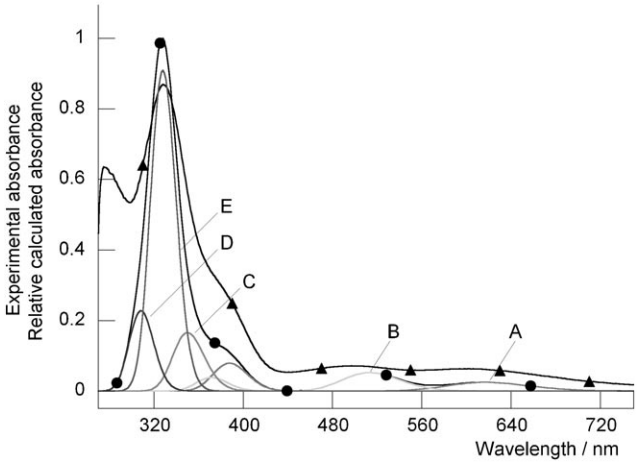

Figure 11. Overlay of the experimental UV/Vis spectrum (▲) of the reduced copper(I) species of **1** with the simulated TD-DFT electronic absorption spectrum (●) of $[Cu^{I}ATSM]^{-}$. Band assignments and MOs are presented in the Supporting Information.

spectrum has been deconvoluted as the sum of Gaussian-shaped bands with a global half-band width ($\Delta_{1/2}$) of 2000 cm^{-1}.[69] Band assignments and MO isosurfaces are given in the Supporting Information. From the combined evidence of the electrochemistry, UV/Vis SEC and TD-DFT calculations, the reduced copper(I) species is assigned as the anionic species $[Cu^{I}ATSM]^{-}$.

EPR SEC: Experimental EPR spectra of complexes **1**–**7** were recorded in anhydrous DMF at room temperature (RT) and 100 K. Simulated EPR parameters are presented in Table 4 and the Supporting Information.[60,70] Copper(II)–bis(thiosemicarbazonato) complexes typically exhibit copper hyperfine splitting of around 91.0 G, with nitrogen superhyperfine coupling constants around 16.0 G and line intensities in a ratio of 1:2:3:2:1. The values derived for **1**, are slightly lower than those found by West et al.[70] and the low g_{iso} value of 2.055, is indicative of the covalent nature of the metal–ligand bonding in these copper(II) complexes.[71] RT solution-phase spectra were simulated with EasySpin by using the fast-motion regime.[72] In the RT simulations, only coupling of the unpaired electron to a copper-63 nucleus was considered. However, copper acetate used in the synthesis was a mixture of copper-63 and copper-65 in natural abundance (69.17 and 30.83%, respectively).[73] These two isotopes have slightly different nuclear magnetic moments of 2.22 and 2.38, respectively, which accounts for the minor differences observed between the experimental and simulated EPR spectra (see the Supporting Information).

Table 4. EPR parameters for the copper(II)–bis(thiosemicarbazonato) complexes **1**–**7**.

	Solution phase[a]			Frozen solution[b]	
	A_{Cu} [G]	A_N [G]	g_{iso}	$A_{Cu}(z)$ [G]	$g(z)$
1	91.0	16.0	2.055	194	2.11
2	92.0	16.0	2.058	192	2.1113
3	92.0	15.5	2.058	192	2.116
4	91.5	15.0	2.059	191	2.1185
5	92.0	16.0	2.058	180	2.132
6	92.0	16.0	2.057	192	2.112
7	70.0	9.0	2.065	155	2.135

[a] DMF at 290 K, ^{63}Cu-only simulations performed using EasySpin. [b] DMF glass at 100 K, simulations performed with ^{63}Cu and ^{65}Cu isotopes in natural abundance using SimFonia. Full EPR parameters are given in the Supporting Information.

Simulations of the frozen solution spectra were performed with copper-63 and copper-65 isotopes in natural abundance by using Bruker Win-EPR SimFonia software (see the Supporting Information).[74] In a plot of $A_{Cu}(z)$ versus $g(z)$, complexes **1**–**6** were found to cluster in the same region, which indicates that in solution these copper(II) complexes have similar electronic and geometric structures.[75] In contrast, complex **7** deviated from this region due to the lower $A_{Cu}(z)$ hyperfine coupling constants of 155 G, respectively. This deviation is assigned to the pseudo-tetrahedral geometry of **7** in solution.

Figure 12 shows the change in EPR signal intensity observed during in situ electrochemical reduction of **1** in anhydrous, deoxygenated DMF. Previously, it was suggested that

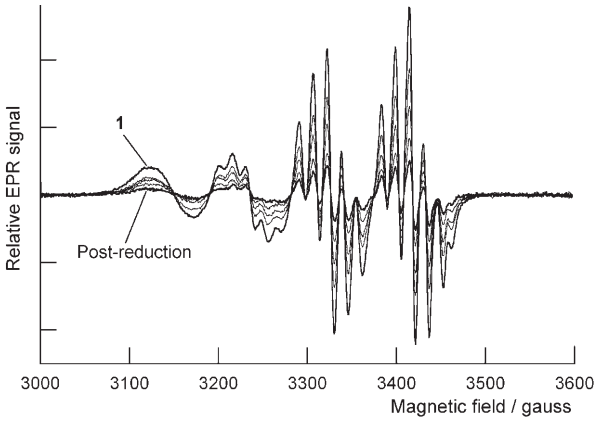

Figure 12. Change in the EPR spectrum of a 1.0×10^{-3} mol dm^{-3} solution of **1** in anhydrous, deoxygenated DMF during electrochemical reduction at $E_{appl}(SCE) = -1.259$ V for 7200 s. A microwave frequency of 9.4493 GHz was used. The relative intensity of the EPR spectrum returned to 93.4% of the initial spectrum 7200 s after electrochemical reduction, due to oxidation by O_2(sol) and diffusion of **1** into the cavity from the bulk solution.

reduction may be ligand-based, leading to the formation of a triplet anionic species.[39,60,76] No evidence of a ligand-based triplet species was observed in the frozen solution spectrum of **1** after electrochemical reduction. These EPR SEC experiments confirm the results of previous calcula-

tions that indicate one-electron reduction of copper(II)–bis-(thiosemicarbazonato) complexes is metal-centred, which leads to the formation of EPR silent, closed-shell copper(I) d^{10} species.[40] They also provide further evidence on the nature of the redox equilibrium between **1** and the reduced copper(I) anion $[Cu^{I}ATSM]^{-}$.

Acid titrations: The microenvironment of tumours is known to be more acidic than normal tissue phenotypes. Both extracellular tissue pH values (pHe), measured by using invasive pH electrodes, and intracellular pH values (pHi), measured in vitro by using pH-sensitive fluorescent dyes, such as the carboxyfluorescein dye, 2′,7′-bis(carboxyethyl)-5(6)-carboxyfluorescein (BCECF),[77,78] and in vivo by using ^{31}P NMR spectroscopy,[79,80] have been show to decrease by around 0.5–1.0 pH units in tumours. Upregulation of the p53 and p21 genes and the production of vascular endothelial growth factor (VEGF), associated with angiogenesis, have been linked to tumour acidosis and hypoxia. Low pH and pO_2 levels also increase tumour metastasis and confer resistance to ionising radiation.[81–85] Therefore, the effect of changing acid concentration and pH on the electrochemistry, UV/Vis and EPR SEC of complexes **1–8** was investigated.

Several new peaks, labelled E/F and P_1–P_4 in Figure 13, were observed in the CVs of **1** on titration with concentrated tetrafluoroboric acid HBF_4 in anhydrous, deoxygenated

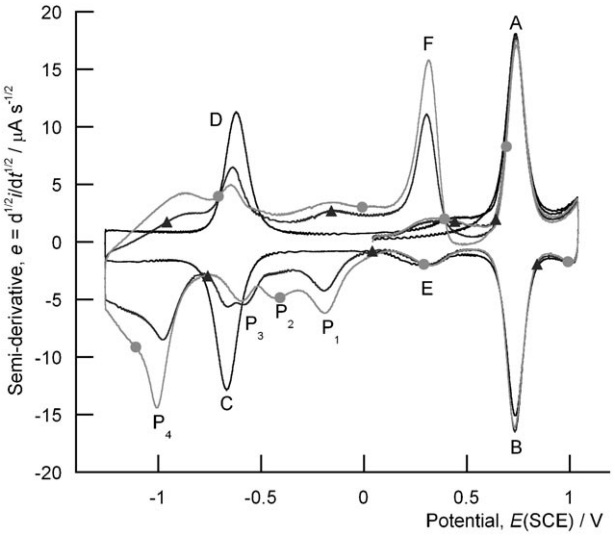

Figure 13. Change in the semi-derivative of the CVs of a 1.0×10^{-3} mol dm^{-3} solution of **1** (——) recorded at 100 mV s^{-1} in anhydrous, deoxygenated DMF on titration with concentrated HBF_4. In the presence of 1 (▲) or 2 equiv (●) of concentrated HBF_4, the new peaks P_1–P_4 are observed. The peak current of the anodic wave F increases with increasing HBF_4 concentration.

DMF at 295 K. The half-wave potential and peak currents of the ligand-based one-electron A/B oxidation couple are unaffected by the presence of strong acids. Therefore, the A/B couple was used as an internal reference. The irreversible reduction processes (P_1–P_4) occur at potentials of −0.191, −0.448, −0.597 and −1.007 V, respectively. These four processes are associated with the solution phase rather than surface-adsorbed species and display typical diffusion controlled (Cottrell) behaviour.

Redox process P_4 is assigned to the reduction of protons to give H_2(g). After prolonged reduction times (>1500 s) of solutions of the copper(II) complexes acidified with concentrated HBF_4 in the OTTLE cell, small bubbles of hydrogen gas were evolved and trapped between the wires of the platinum mini-grid. Process P_3 is observed in the CVs of background experiments of concentrated HBF_4 in anhydrous, deoxygenated DMF in the absence of copper(II) complexes, and is assigned to an impurity (possibly hydrogen fluoride) present in the concentrated HBF_4 sample.

Redox process P_1 is assigned to an irreversible one-electron reduction in which $W_{pc}=144$ mV, $n_c=1.05$ and $\alpha=0.52$.[53] The species associated with P_1 is present at low concentrations of concentrated HBF_4 and appears after only 0.25 equivalents of acid are titrated into the solution. In contrast, process P_2, which also corresponds to a one-electron reduction, requires higher concentrations of strong acids (>1.2 equiv of concentrated HBF_4) before the peak develops.

In the presence of strong non-coordinating acids, it is likely that protonated equilibria account for the species associated with processes P_1 and P_2. Both cathodic and anodic peak currents of the C/D redox couple decrease with increasing concentration of concentrated HBF_4. However, the half-wave potential remains constant at −0.646 V. If the reduction mechanism was a sequential electrochemical–chemical (EC) scheme, the peak currents of the C/D redox couple would be expected to remain constant in the presence of acid. Therefore, the data supports a pre-equilibrium between different protonated species, and the reduction mechanism in the presence of acid is assigned to a sequential chemical–electrochemical ($C_{rev}E_{rev}$) scheme.

Process P_1 is assigned to the one-electron reduction of $[Cu^{II}ATSMH]^{+}$. Although reduction of P_1 is formally irreversible, a very small anodic wave is observed on the return sweep that corresponds to oxidation of $[Cu^{I}ATSMH]$. Process P_2 occurs at a more negative reduction potential than P_1 and is tentatively assigned to the one-electron reduction of $[Cu^{II}ATSMH_2]^{2+}$. The appearance of P_2 only at acid concentrations >1.2 equivalents supports this conclusion. However, it is also possible that diprotonation facilitates the formation of loosely coordinated copper(II) dimeric species, which may account for the shift to a more negative reduction potential.[60]

In the absence of acid, the E/F redox couple (Figures 2 and 13) is present with a half-wave potential value of +0.319 V, but only gives rise to very low peak currents. On addition of strong acids, the anodic current of peak F increases, whereas the peak current of E remains constant. The peak current of F remains low if the reduction processes P_1, P_2 and C/D are excluded from the cyclic voltammetry sweep width (see the Supporting Information). If the sweep

width is increased to include potentials more negative than process P_1, the peak current associated with F increases. From the peak shape it can be concluded that oxidative process F does not display typical diffusion controlled behaviour and is characteristic of a stripping voltammetry peak.[55] In addition, the semi-derivative peak current (e_{pa}) of process F continues to increase on successive cyclic voltammetry cycles. The same process was also observed when a platinum microdisc electrode was used.

Therefore, the electroactive species associated with F is electrodeposited on the surface of the electrode at deposition potentials (E_d) of < -0.191 V. Electrodeposition was confirmed by further cyclic voltammetry experiments (see the Supporting Information). From a half-peak width value of 94 mV, the number of electrons transferred and the transfer coefficient were calculated to be $n_a = 1.98$ and $\alpha = 0.40$. Background CVs of the proligand of **1** (H_2ATSM) with and without concentrated HBF_4 showed no Faradaic processes at the potential of the E/F redox couple. These experiments show that ligand dissociation is slow on the cyclic voltammetry timescale.

One-electron reduction of the solution-phase species associated with processes P_1, P_2 and the C/D redox couple lead to electrodeposition of a common copper(I) species on the surface of the electrode. The invariance of the A/B redox couple indicates that the deposited species is stripped from the surface to give the neutral species **1** in solution. Based on the calculated number of electrons transferred, the electroactive species associated with peak F is assigned to the two-electron oxidation of the dimeric copper(I) species **1d** (Figure 5).

When electrochemistry experiments were performed with the weaker acetic acid, no change was observed in the CV of **1**. However, similar electrochemical behaviour to that described for complex **1** in the presence of concentrated HBF_4 was observed for complexes **2**–**4**.[39] Previous DFT calculations of absolute pK_a values indicate that the cationic, monoprotonated species ($[Cu^{II}LH]^+$) of **2**–**4** are less acidic than $[Cu^{II}ATSMH]^+$.[40] Therefore, complexes **2**–**4** are likely to protonate more readily and are reduced at less negative potentials.

An overlay of the UV/Vis spectra of **1**, H_2ATSM, and the changes observed before and after electrochemical reduction in deoxygenated DMF acidified with concentrated HBF_4 is shown in Figure 14. The addition of concentrated HBF_4 leads to a blueshift of around 14 nm in the metal-to-ligand charge-transfer bands to 464 nm, and an overall decrease in absorbance above 300 nm.[41] This supports the conclusion that in the presence of strong acids protic equilibria are established between **1** and the mono- and diprotonated cationic species.

Figure 15 shows the time-dependent change in absorbance at 334 nm during the reduction of **1** in the presence of concentrated HBF_4. An initial decrease in absorbance is observed at the start of the electrochemical reduction at -1.051 V (point A). At point B, the absorbance begins to increase due to dissociation of the copper(I) ion from the protonated H_2ATSM ligand. During the time between points B and D, two isosbestic points are observed in the UV/Vis spectrum at 371 and 297 nm. An overlay of the UV/Vis spectrum of H_2ATSM generated during electrochemical reduction in acidified DMF and one equivalent of the proligand in DMF (Figure 14) reveals that on the SEC timescale, quantitative reduction and ligand dissociation occurs (Figure 15 point C). When the potentiostat is switched to open circuit (point D), an immediate, and very rapid decrease in the absorbance at 334 nm occurs (point E). The final spectrum, recorded at point F, does not correspond to either the spectrum of **1** or the protonated copper(II) species. It is likely that the copper(I) ion released into solution (presumably as $[Cu(DMF)_4]^+$) will be reoxidised at the working electrode. The rapid loss of absorbance at point D (Figure 15) may be due to subsequent solution-phase redox

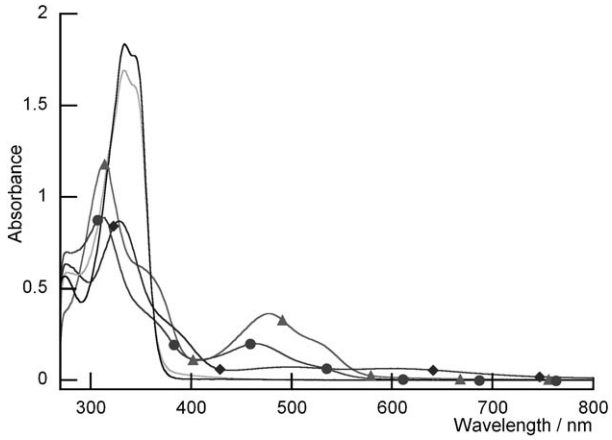

Figure 14. Overlay of the UV/Vis spectra of **1** (▲), the reduced copper species $[Cu^{I}ATSM]^-$ (♦), the final spectrum of **1** recorded during electrochemical reduction of **1** in the presence of concentrated HBF_4 (●), the H_2ATSM proligand (——) and H_2ATSM obtained from the reduction of **1** (——).

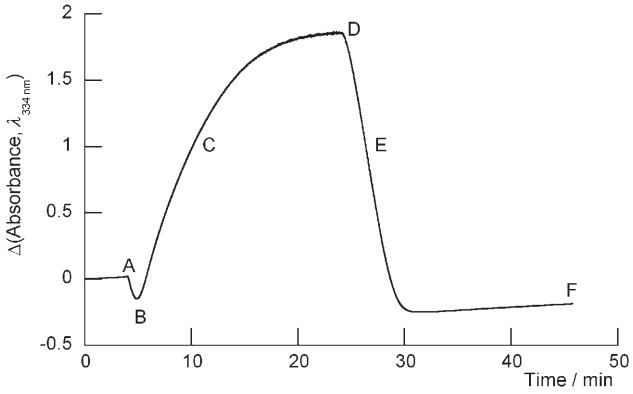

Figure 15. Time-resolved change observed in the experimental UV/Vis peak absorbance at 334 nm during the electrochemical reduction of a 1.0×10^{-3} mol dm^{-3} solution of **1** in deoxygenated DMF acidified with concentrated HBF_4 during electrochemical reduction at E_{appl}(SCE) = -1.051 V. Labels A–F are discussed in the main text.

reactions occurring between H_2ATSM and the Cu^{II}/Cu^{I} ions in acidic solution.

Changes in the UV/Vis and EPR spectra of **1** upon titration with acidic solutions of HBF_4, $HClO_4$, acetic acid, HCl, HBr and HI in DMF were measured (see the Supporting Information). In the presence of small amounts of strong acids, HBF_4, $HClO_4$ and HPF_6, the UV/Vis spectrum of **1** changes to give the same spectrum as shown in Figure 14. No change was observed on titration of **1** with acetic acid, and interestingly, no change occurred when an excess of the biologically ubiquitous reducing agent glutathione (GSH) was added both separately and to the solution of **1** acidified with concentrated HBF_4.[86,87] This indicates that GSH alone is not able to reduce **1**.

Addition of HCl and HBr leads to the formation of new EPR-active species with an associated change in the UV/Vis spectra (see the Supporting Information). Reaction of HCl and HBr with **1** may lead to the formation of mono- and/or diprotonated complexes with halide anions coordinated to the copper(II) ion in the axial sites. On addition of concentrated HI, the EPR signal is lost and the UV/Vis spectrum changes slowly over 10 min to give the spectrum of H_2ATSM. No change in either the UV/Vis or EPR spectra of **1** are observed on addition of NaI. However, if concentrated HBF_4 is then added to the solution of **1** with NaI, the same result as that for the titration with concentrated HI is observed.

These results demonstrate that iodide anions are not able to reduce **1**. However, in the presence of strong acids, iodide anions are capable of reducing the mono- or diprotonated copper(II) species $[Cu^{II}ATSMH]^+$ and $[Cu^{II}ATSMH_2]^{2+}$. Copper(I) iodide is soluble in DMF, and consequently, does not precipitate from solution. Acetic acid is too weak to protonate **1** in DMF and no change occurs in either the UV/Vis or EPR spectra on titration.

Discussions on the mechanism of hypoxia selectivity: Over recent years, several research groups have investigated the reductive retention of **1** and two mechanisms of hypoxia selectivity have emerged. The first mechanism was proposed by Fujibayashi et al.[25] They suggested that **1** becomes irreversibly trapped upon intracellular reduction that only occurs in hypoxic cells. Experiments showed that $[^{62}Cu^{II}ATSM]$ accumulates in hypoxic myocardium through a bioreductive retention mechanism involving nicotinimide adenine dinucleotide (NADH) dependent mitochondrial enzymes of the electron-transport chain (ETC).[25,88] Subsequently, Obata et al.[38] showed that in subcellular fractions of Erhlich ascites tumour cells, reduction of **1** is mediated by enzymes located in the microsome/cytosol fraction, rather than the mitochondria. Reduction of **1** was found to be heat sensitive and was enhanced by the addition of both NADH and nicotinimide adenine dinucleotide phosphate (NADPH) to the medium. Neither NADH nor NADPH are capable of reducing **1** alone. Specific reductase inhibitor studies also showed that in comparison with control experiments, inhibition of the microsomal enzymes, NADH-dependent cytochrome b5 reductase and NADPH-dependent cytochrome P450 reductase, by phenylthiourea (PTU) and adenosine monophosphate (AMP), respectively, caused a 25–50% decrease in the reduction of **1**.

However, this first mechanism is inconsistent with cellular uptake and washout studies, which led to the proposal of a second mechanism by Dearling et al.[36,37] and Maurer et al.[39] They suggested that reduction of **1** is reversible and occurs in both hypoxic and normoxic cells, generating the unstable, anionic copper(I) complex $[Cu^{I}ATSM]^-$. It was suggested that this species may dissociate slowly in hypoxic cells, which leads to irreversible trapping of the copper ion. In the presence of normal oxygen tensions, the $[Cu^{I}ATSM]^-$ anion is reoxidised to the neutral copper(II) complex, which can diffuse out of the cells. In this mechanism, the relative stability of the reduced copper(I) anion with respect to ligand dissociation is the discriminating factor between the hypoxia-selective complex **1** and the non-selective blood perfusion tracer complex **2**.[89]

A revised mechanism that builds upon the work of Dearling et al. and is consistent with the electrochemistry, SEC, DFT calculations and observed cellular uptake experiments is shown in Scheme 2.[36,37] Although the mechanism of cellular uptake is uncertain given the low molecular weight, high lipophilicity (log *P*) and planarity of complexes **1**–**6**, it is plausible that cellular uptake may occur by passive diffusion. Once inside the cell, NADH/NADPH-dependent enzyme-mediated reduction is likely to occur for all copper(II)–bis(thiosemicarbazonato) complexes in both normoxic and hypoxic tissue. Although caution must be applied when extrapolating between the chemical results in DMF and biological systems, the electrochemistry experiments show that reduction generates a copper(I) anionic species, for example, $[Cu^{I}ATSM]^-$ or $[Cu^{I}PTSM]^-$. In the absence of acid this anionic species is stable with respect to ligand dissociation. This result represents a departure from the second mechanism proposed, and therefore, the intracellular trapping and hypoxia selectivity must originate from another aspect of the chemistry of these complexes.[36,37]

We propose that the relative rates of oxidation and acid-catalysed dissociation of the copper(I) anionic species, and the position of equilibria between protonated species, are crucial to the mechanism of hypoxia selectivity. SEC experiments and DFT calculations show that complexes with more negative one-electron reduction potentials are more readily oxidised by dioxygen than complexes with less negative reduction potentials. For example, complex **1** is harder to reduce than complex **2**, and the copper(I) anion $[Cu^{I}ATSM]^-$ is oxidised back to the neutral complex **1** more rapidly than the $[Cu^{I}PTSM]^-$ anion. However, in the absence of acid, both anions are stable to ligand dissociation on the relatively long timescale of the UV/Vis SEC experiments.

The reduction potentials and pK_a values of complexes **1**–**4** depend on the electron-donating nature of the substituents on the ligand backbone.[40] The calculations and experiments described herein show that the conjugate acids of complexes

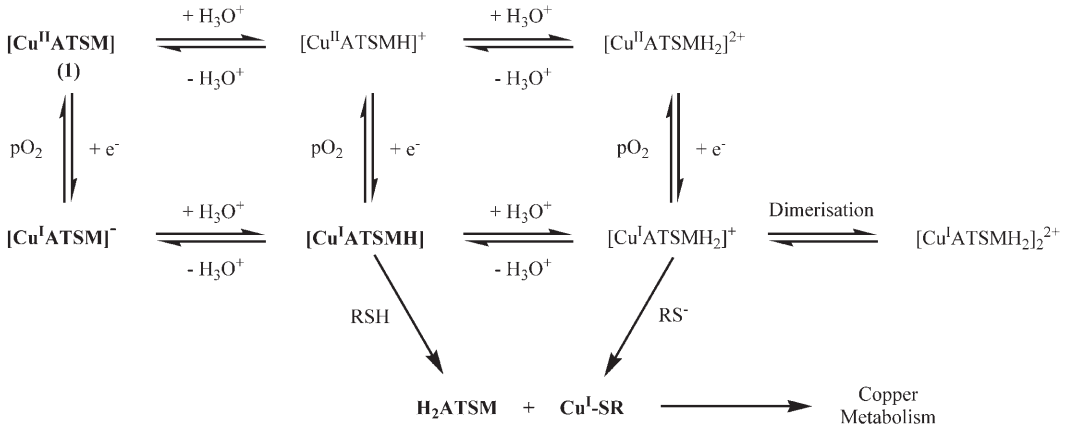

Scheme 2. Diagram of the proposed mechanism of reduction and protonation of **1** and related copper(II)–bis(thiosemicarbazonato) complexes (Scheme 1). The mechanism can be used to account for the observed differences in hypoxia selectivity between complexes **1** and **2**. The species shown in bold represent a plausible pathway for intracellular reduction. However, the other species, including the copper(I) dimer, are unlikely to be found in the cellular environment.

with either one or two hydrogen substituents at the R_1 and R_2 positions are less acidic than the conjugate acid of **1**. Therefore, in comparison with the non-hypoxia selective complex **2**, the position of equilibrium between **1** and the copper(I) anion is displaced further towards the neutral copper(II) complex. In addition, for complex **1** the position of the equilibria established between the protonated and non-protonated forms of both the copper(II) and copper(I) species lie towards the non-protonated complexes. In contrast, complex **2** is more readily reduced and more easily protonated. Therefore, the position of equilibria is displaced towards the more heavily protonated, reduced copper(I) species of complex **2**, increasing the propensity for ligand dissociation and leading to irreversible trapping of the corresponding proligand and copper(I) ions.

The revised mechanism (Scheme 2) is fully consistent with cellular uptake and washout studies.[36,37] Non-steady-state kinetic modelling with the mechanism developed herein and the cellular uptake and washout data reported by Lewis et al. has also been conducted.[90] Full results will be reported elsewhere. However, the mechanism was found to be in excellent agreement with the experimental data, with an overall calculated variance between the experimental and simulated uptake profiles of $<7\%$, which lies within experimental error (see the Supporting Information).

All copper(II)–bis(thiosemicarbazonato) complexes are taken up by both normoxic and hypoxic cells in which intracellular enzyme-mediated reduction, generating copper(I) anionic species, occurs. In normoxic cells, rapid and facile oxidation of $[Cu^{I}ATSM]^{-}$ coupled with the low pK_a of the conjugate acid means that the position of the equilibrium is displaced towards the neutral copper(II) complex. In contrast, for complex **2**, the position of the equilibrium in normoxic cells will be displaced towards the reduced copper(I) protonated species. This increased intracellular concentration of $[Cu^{I}PTSMH]$ and $[Cu^{I}PTSMH_2]^{+}$ increases the rate of ligand dissociation. Therefore, in normoxic cells, complex **2** is more likely to become irreversibly trapped than complex **1**, which is consistent with the higher observed washout concentration of complex **1** from normoxic cells.[36,37] As oxygen tension decreases, the position of the equilibrium of **1** is displaced towards the copper(I) anionic species. In hypoxic cells the more acidic environment means that protonation is more likely to occur, which leads to increased ligand dissociation and irreversible trapping of **1**.

Conclusions

The mechanism of hypoxia selectivity of copper(II)–bis(thiosemicarbazonato) complexes has been investigated by using a range of chemical, electrochemical, spectroscopic and computational methods. Earlier mechanisms focused on the structural dependence of the one-electron Cu^{II}/Cu^{I} reduction, and the relative stability of the reduced copper(I) anionic species towards dissociation as the primary molecular feature governing hypoxia-selective cellular uptake and retention.[25,36–39] Under normoxic conditions, reduction was proposed to be either non-feasible[25,38] or reversible,[36,37,39] with dioxygen thought to be acting as the oxidant for the one-electron oxidation of the reduced copper(I) species. The role of pK_a and protonation of both the copper(II) and reduced copper(I) species was not considered explicitly.

The results presented herein suggest that reduction of copper(II)–bis(thiosemicarbazonato) complexes is highly pH dependent. Dioxygen has been shown to be capable of oxidising the reduced copper(I) species, which, in the absence of a proton source, is stable towards ligand dissociation. A revised mechanism consistent with all available experimental data has been developed and can be used to understand observed differences in the hypoxia selectivity of **1** and $[Cu^{II}PTSM]$. Reduction has been shown to generate the copper(I) anionic species that may undergo oxidation by dioxygen, protonation or ligand dissociation. The position of

the equilibrium between different protonated species is dependent upon the electron-donating/withdrawing nature of the R_1 and R_2 substituents of the chelating ligand. The hypoxia selectivity of **1** arises from a delicate balance between enzyme-mediated one-electron reduction and subsequent reoxidation by dioxygen, versus protonation and ligand dissociation. The revised mechanism may have important implications in the design of new copper-based radiopharmaceuticals.

Experimental Section

General: All reagents and solvents were obtained from commercial sources (SigmaAldrich and Lancaster) and unless otherwise stated were used as received. Elemental analyses were performed by the microanalysis service department at the University of Oxford. NMR spectra were recorded on a Varian Mercury VX300 spectrometer (^{1}H at 300 MHz, ^{13}C{^{1}H} at 75.5 MHz) by using the residual solvent signal as an internal reference. Mass spectra were recorded on a Micromass LCT time-of-flight mass spectrometer by using positive ion electrospray (ES^+) ionisation. When possible accurate masses are reported to four decimal places by using tetraoctylammonium bromide (466.5352 Da) as an internal reference. UV/Vis spectra were recorded on a Perkin–Elmer Lambda 19 UV/Vis/near-IR spectrometer. EPR spectra were recorded by using quartz flat cells 1 or 2 mm thick on a Bruker EMX-micro X-band spectrometer at the EPSRC National EPR Service at the University of Manchester. EPR simulations were performed by using either EasySpin[72] or Bruker Win-EPR SimFonia version 1.26beta software.[74] High-performance liquid chromatography (HPLC) was conducted by using a Gilson HPLC machine equipped with a Hamilton PRP-1 reverse-phase column and UV/Vis detection at 254 nm. Retention times obtained by using a water/acetonitrile gradient elution method (shown in the Supporting Information) are presented for all compounds. Calculated lipophilicities (log P_c values) have been estimated from the HPLC retention times and calibration of the apparatus by using experimental water/octanol partition coefficients of complexes **1–6** reported in the literature.[37]

Electrochemistry experiments were performed by using a CH Instruments Electrochemical Analyser. The potentiostat was controlled using a PC running CH Instruments version 2.05 electrochemical software. All cyclic voltammetry measurements were recorded in a glass cell sealed with a Teflon cap and located inside a Faraday cage at a temperature of (21.5 ± 1.5) °C. Further details are given in the Supporting Information.

UV/Vis SEC experiments were performed in anhydrous DMF with 0.1 mol dm^{-3} TBA-BF_4 as a supporting electrolyte by using a custom-made optically transparent thin-layer electrode (OTTLE) quartz cell (path length, $l = 0.46$ mm), sealed with a Teflon cap. The total volume of the OTTLE cell was approximately 4 mL. The same auxiliary and reference electrodes as those used in the cyclic voltammetry measurements were situated in the bulk solution above the cavity and a platinum wire mesh (approximately 50 wires per inch, 0.10 mm thick) located inside the cavity was used as the working electrode. A similar experimental design was used for the EPR SEC measurements.

Synthesis: Bis(thiosemicarbazone) proligands and the corresponding copper(II)–bis(thiosemicarbazonato) complexes, **1–9**, were synthesised in accordance with previously reported procedures.[45,47] All characterisation data was found to be consistent with the proposed structures. Full details are given in the Supporting Information.

DFT calculations: All calculations were conducted using DFT[91,92] as implemented in the Gaussian 03 suite of ab initio quantum chemistry programs.[68] Geometry optimisations and vibrational frequency calculations were performed by using the unrestricted uB3LYP exchange and correlation functionals and the double-ζ 6-31++G(d,p) basis set for all atoms. Full computational details are given in the Supporting Information. A more detailed description of the calculations has been given previously.[40]

X-ray crystallography: Crystals of complexes **7–9** were mounted on a glass fibre and cooled rapidly to 150 K in a stream of cold N_2 by using an Oxford Cryosystems CRYOSTREAM unit. Diffraction data was measured by using an Enraf-Nonius Kappa CCD diffractometer (graphite-monochromated $Mo_{K\alpha}$ radiation, $\lambda = 0.71073$ Å). Intensity data was processed using the DENZO-SMN package.[93]

Space groups were identified by examination of the systematic absences in the intensity data. The structures were solved by using the direct methods program SIR92,[94] which located all non-hydrogen atoms. Subsequent full-matrix least-squares refinement was carried out by using the CRYSTALS program suite.[95] Coordinates and anisotropic thermal parameters of all non-hydrogen atoms were refined. The NH hydrogen atoms were located in the difference Fourier map and their coordinates and isotropic thermal parameters were subsequently refined. Other hydrogen atoms were positioned geometrically after each cycle of refinement. A three-term Chebychev polynomial weighting scheme was applied.

CCDC-682479 (**7**), 682480 (**8**) and 682481 (**9**) contain the supplementary crystallographic data for this paper. This data can be obtained free of charge from The Cambridge Crystallographic Data Centre via www.ccdc.cam.ac.uk/data_request/cif.

Acknowledgements

Thanks are due to all members of the Dilworth and Green groups at the University of Oxford. J.P.H. thanks Merton College and the EPSRC for a studentship. Complexes **7–9** were a gift from Prof. R. S. McElhinney, Trinity College, Dublin, and we thank Prof. T. B. H. McMurry and Dr. T. McCabe. We thank Prof. A. M. Bond for helpful discussions. We are indebted to Prof. D. J. Watkin, Dr. N. Rees, Dr. A. R. Cowley, Dr. A. Thompson, C. Sparrow and M. Marshall for technical support. We also thank the Oxford Supercomputing Centre.

[1] B. Blouw, H. Song, T. Tihan, J. Bosze, N. Ferrara, H.-P. Gerber, R. S. Johnson, G. Bergers, *Cancer Cell* **2003**, *4*, 133.
[2] D. A. Chan, A. J. Giaccia, *Cancer Metastasis Rev.* **2007**, *26*, 333.
[3] J. M. Brown, *Cancer Res.* **1999**, *59*, 5863.
[4] J. M. Brown, W. R. Wilson, *Nat. Rev. Cancer* **2004**, *4*, 437.
[5] J. L. Tatum, G. J. Kelloff, R. J. Gillies, J. M. Arbeit, J. M. Brown, K. S. C. Chao, J. D. Chapman, W. C. Eckelman, A. W. Fyles, A. J. Giaccia, R. P. Hill, C. J. Koch, M. C. Krishna, K. A. Krohn, J. S. Lewis, R. P. Mason, G. Melillo, A. R. Padhani, G. Powis, J. G. Rajendran, R. Reba, S. P. Robinson, G. L. Semenza, H. M. Swartz, P. Vaupel, D. Yang, B. Croft, J. Hoffman, G. Liu, H. Stone, D. Sullivan, *Int. J. Radiat. Biol.* **2006**, *82*, 699.
[6] L. H. Gray, A. D. Conger, M. Ebert, S. Hornsey, O. C. A. Scott, *Br. J. Radiol.* **1953**, *26*, 638.
[7] R. H. Thomlinson, L. H. Gray, *Br. J. Cancer* **1955**, *9*, 539.
[8] M. Rudin, R. Weissleder, *Nat. Rev. Drug Discovery* **2003**, *2*, 123.
[9] M. E. Phelps, *Proc. Natl. Acad. Sci. USA* **2000**, *97*, 9226.
[10] L. I. Wiebe, *Int. Congr. Ser.* **2004**, *1264*, 53.
[11] J. S. Lewis, M. J. Welch, *Q. J. Nucl. Med.* **2001**, *45*, 183.
[12] S. V. Smith, *J. Inorg. Biochem.* **2004**, *98*, 1874.
[13] P. J. Blower, J. S. Lewis, J. Zweit, *Nucl. Med. Biol.* **1996**, *23*, 957.
[14] M. F. Adam, E. C. Gabalski, D. A. Bloch, J. W. Oehlert, J. M. Brown, A. A. Elsaid, H. A. Pinto, D. J. Terris, *Head Neck J. Sci. Spec.* **1999**, *21*, 146.
[15] D. M. Brizel, G. S. Sibley, L. R. Prosnitz, R. L. Scher, M. W. Dewhirst, *Int. J. Radiat. Oncol. Biol. Phys.* **1997**, *38*, 285.
[16] W. A. Volkert, T. J. Hoffman, *Chem. Rev.* **1999**, *99*, 2269.
[17] S. S. Jurisson, J. D. Lydon, *Chem. Rev.* **1999**, *99*, 2205.
[18] P. Blower, *Dalton Trans.* **2006**, 1705.

[19] L. S. Ziemer, S. M. Evans, A. V. Kachur, A. L. Shuman, C. A. Cardi, W. T. Jenkins, J. S. Karp, A. Alavi, W. R. Dolbier, Jr., C. J. Koch, *Eur. J. Nucl. Med. Mol. Imaging* **2003**, *30*, 259.
[20] O. Couturier, A. Luxen, J.-F. Chatal, J.-P. Vuillez, P. Rigo, R. Hustinx, *Eur. J. Nucl. Med. Mol. Imaging* **2004**, *31*, 1182.
[21] J. M. Brown, *Drug Resist. Updates* **2000**, *3*, 7.
[22] K. B. Peters, J. M. Brown, *Cancer Res.* **2002**, *62*, 5248.
[23] J. R. Dilworth, S. J. Parrott, *Chem. Soc. Rev.* **1998**, *27*, 43.
[24] P. J. Blower, J. R. Dilworth, R. I. Maurer, G. E. D. Mullen, C. A. Reynolds, Y. Zheng, *J. Inorg. Biochem.* **2001**, *85*, 15.
[25] Y. Fujibayashi, H. Taniuchi, Y. Yonekura, H. Ohtani, J. Konishi, A. Yokoyama, *J. Nucl. Med.* **1997**, *38*, 1155.
[26] A. L. Vavere, J. S. Lewis, *Dalton Trans.* **2007**, 4893.
[27] N. Takahashi, Y. Fujibayashi, Y. Yonekura, J. Welch Michael, A. Waki, T. Tsuchida, N. Sadato, K. Sugimoto, H. Itoh, *Ann. Nucl. Med.* **2000**, *14*, 323.
[28] F. Dehdashti, W. Grigsby Perry, A. Mintun Mark, S. Lewis Jason, A. Siegel Barry, J. Welch Michael, *Int. J. Radiat. Oncol. Biol. Phys.* **2003**, *55*, 1233.
[29] F. Dehdashti, M. A. Mintun, J. S. Lewis, J. Bradley, R. Govindan, R. Laforest, M. J. Welch, B. A. Siegel, *Eur. J. Nucl. Med. Mol. Imaging* **2003**, *30*, 844.
[30] K. S. C. Chao, W. R. Bosch, S. Mutic, S. Lewis Jason, F. Dehdashti, A. Mintun Mark, J. F. Dempsey, C. A. Perez, J. A. Purdy, J. Welch Michael, *Int. J. Radiat. Oncol. Biol. Phys.* **2001**, *49*, 1171.
[31] J. A. O'Donoghue, P. Zanzonico, A. Pugachev, B. Wen, P. Smith-Jones, S. Cai, E. Burnazi, R. D. Finn, P. Burgman, S. Ruan, J. S. Lewis, M. J. Welch, C. C. Ling, J. L. Humm, *Int. J. Radiat. Oncol. Biol. Phys.* **2005**, *61*, 1493.
[32] H. Yuan, T. Schroeder, J. E. Bowsher, L. W. Hedlund, T. Wong, M. W. Dewhirst, *J. Nucl. Med.* **2006**, *47*, 989.
[33] P. W. Grigsby, R. S. Malyapa, R. Higashikubo, J. K. Schwarz, M. J. Welch, P. C. Huettner, F. Dehdashti, *Mol. Imaging Biol.* **2007**, *9*, 278.
[34] F. Dehdashti, P. W. Grigsby, J. S. Lewis, R. Laforest, B. A. Siegel, M. Welch, *J. Nucl. Med.* **2008**, *49*, 201.
[35] A. Obata, S. Kasamatsu, J. S. Lewis, T. Furukawa, S. Takamatsu, J. Toyohara, T. Asai, M. J. Welch, S. G. Adams, H. Saji, Y. Yonekura, Y. Fujibayashi, *Nucl. Med. Biol.* **2005**, *32*, 21.
[36] J. L. J. Dearling, J. S. Lewis, D. W. McCarthy, M. J. Welch, P. J. Blower, *Chem. Commun.* **1998**, 2531.
[37] J. L. J. Dearling, J. S. Lewis, G. E. D. Mullen, M. J. Welch, P. J. Blower, *J. Biol. Inorg. Chem.* **2002**, *7*, 249.
[38] A. Obata, E. Yoshimi, A. Waki, J. S. Lewis, N. Oyama, M. J. Welch, H. Saji, Y. Yonekura, Y. Fujibayashi, *Ann. Nucl. Med.* **2001**, *15*, 499.
[39] R. I. Maurer, P. J. Blower, J. R. Dilworth, C. A. Reynolds, Y. Zheng, G. E. D. Mullen, *J. Med. Chem.* **2002**, *45*, 1420.
[40] J. P. Holland, J. C. Green, J. R. Dilworth, *Dalton Trans.* **2006**, 783.
[41] J. P. Holland, F. I. Aigbirhio, H. M. Betts, P. D. Bonnitcha, P. Burke, M. Christlieb, G. C. Churchill, A. R. Cowley, J. R. Dilworth, P. S. Donnelly, J. C. Green, J. M. Peach, S. R. Vasudevan, J. E. Warren, *Inorg. Chem.* **2007**, *46*, 465.
[42] B. A. Gingras, R. W. Hornal, C. H. Bayley, *Can. J. Chem.* **1960**, *38*, 712.
[43] B. A. Gingras, R. L. Somorjai, C. H. Bayley, *Can. J. Chem.* **1961**, *39*, 973.
[44] B. A. Gingras, T. Suprunchuk, C. H. Bayley, *Can. J. Chem.* **1962**, *40*, 1053.
[45] M. Christlieb, J. R. Dilworth, *Chem. Eur. J.* **2006**, *12*, 6194.
[46] P. J. Blower, T. C. Castle, A. R. Cowley, J. R. Dilworth, P. S. Donnelly, E. Labisbal, F. E. Sowrey, S. J. Teat, M. J. Went, *Dalton Trans.* **2003**, 4416.
[47] M. Gannon, J. E. McCormick, R. S. McElhinney, *Proc. R. Ir. Acad. Sect. B.* **1980**, *80B*, 117.
[48] L. J. Farrugia, *J. Appl. Crystallogr.* **1997**, *30*, 565.
[49] R. S. Cahn, C. Ingold, V. Prelog, *Angew. Chem.* **1966**, *78*, 413; *Angew. Chem. Int. Ed. Engl.* **1966**, *5*, 385.
[50] A. R. Cowley, J. Davis, J. R. Dilworth, P. S. Donnelly, R. Dobson, A. Nightingale, J. M. Peach, B. Shore, D. Kerr, L. Seymour, *Chem. Commun.* **2005**, 845.
[51] J. C. Imbeaux, J. M. Saveant, *J. Electroanal. Chem. Interfacial Electrochem.* **1973**, *44*, 169.
[52] A. M. Bond, T. L. Henderson, K. B. Oldham, *J. Electroanal. Chem. Interfacial Electrochem.* **1985**, *191*, 75.
[53] P. Dalrymple-Alford, M. Goto, K. B. Oldham, *J. Electroanal. Chem. Interfacial Electrochem.* **1977**, *85*, 1.
[54] P. Dalrymple-Alford, M. Goto, K. B. Oldham, *Anal. Chem.* **1977**, *49*, 1390.
[55] A. J. Bard, L. R. Faulkner . *Electrochemical Methods: Fundamentals and Applications*, 2nd Edition, Wiley, New York, **2001**.
[56] S. R. Jacob, Q. Hong, B. A. Coles, R. G. Compton, *J. Phys. Chem. B* **1999**, *103*, 2963.
[57] M. Rudolph, D. P. Reddy, S. W. Feldberg, *Anal. Chem.* **1994**, *66*, 589A.
[58] A. R. Cowley, J. R. Dilworth, P. S. Donnelly, E. Labisbal, A. Sousa, *J. Am. Chem. Soc.* **2002**, *124*, 5270.
[59] T. P. DeAngelis, W. R. Heineman, *J. Chem. Educ.* **1976**, *53*, 594.
[60] L. E. Warren, S. M. Horner, W. E. Hatfield, *J. Am. Chem. Soc.* **1972**, *94*, 6392.
[61] D. L. Maricle, W. G. Hodgson, *Anal. Chem.* **1965**, *37*, 1562.
[62] M. E. Peover, B. S. White, *Electrochim. Acta* **1966**, *11*, 1061.
[63] H. J. James, R. F. Broman, *J. Phys. Chem.* **1971**, *75*, 4019.
[64] D. Vasudevan, H. Wendt, *J. Electroanal. Chem.* **1995**, *392*, 69.
[65] T. W. Kensler, D. M. Bush, W. J. Kozumbo, *Science* **1983**, *221*, 75.
[66] K. Wada, Y. Fujibayashi, N. Tajima, A. Yokoyama, *Biol. Pharm. Bull.* **1994**, *17*, 701.
[67] K. Wada, Y. Fujibayashi, A. Yokoyama, *Arch. Biochem. Biophys.* **1994**, *310*, 1.
[68] Gaussian 03, Revision C.02 or D.01, M. J. Frisch, G. W. Trucks, H. B. Schlegel, G. E. Scuseria, M. A. Robb, J. R. Cheeseman, J. A. Montgomery, Jr., T. Vreven, K. N. Kudin, J. C. Burant, J. M. Millam, S. S. Iyengar, J. Tomasi, V. Barone, B. Mennucci, M. Cossi, G. Scalmani, N. Rega, G. A. Petersson, H. Nakatsuji, M. Hada, M. Ehara, K. Toyota, R. Fukuda, J. Hasegawa, M. Ishida, T. Nakajima, Y. Honda, O. Kitao, H. Nakai, M. Klene, X. Li, J. E. Knox, H. P. Hratchian, J. B. Cross, V. Bakken, C. Adamo, J. Jaramillo, R. Gomperts, R. E. Stratmann, O. Yazyev, A. J. Austin, R. Cammi, C. Pomelli, J. W. Ochterski, P. Y. Ayala, K. Morokuma, G. A. Voth, P. Salvador, J. J. Dannenberg, V. G. Zakrzewski, S. Dapprich, A. D. Daniels, M. C. Strain, O. Farkas, D. K. Malick, A. D. Rabuck, K. Raghavachari, J. B. Foresman, J. V. Ortiz, Q. Cui, A. G. Baboul, S. Clifford, J. Cioslowski, B. B. Stefanov, G. Liu, A. Liashenko, P. Piskorz, I. Komaromi, R. L. Martin, D. J. Fox, T. Keith, M. A. Al-Laham, C. Y. Peng, A. Nanayakkara, M. Challacombe, P. M. W. Gill, B. Johnson, W. Chen, M. W. Wong, C. Gonzalez, J. A. Pople, Gaussian, Inc., Wallingford CT, **2004**.
[69] S. I. Gorelsky, SWizard program, http://www.sg-chem.net/, Department of Chemistry, York University, Toronto, ON (Canada), **1998**.
[70] D. X. West, J. S. Ives, G. A. Bain, A. E. Liberta, J. Valdes-Martinez, K. H. Ebert, S. Hernandez-Ortega, *Polyhedron* **1997**, *16*, 1895.
[71] D. Kivelson, R. Neiman, *J. Chem. Phys.* **1961**, *35*, 149.
[72] S. Stoll, A. Schweiger, *J. Magn. Reson.* **2006**, *178*, 42.
[73] F. H. Allen, O. Kennard, D. G. Watson, L. Brammer, A. G. Orpen, R. Taylor, *J. Chem. Soc. Perkin Trans. 2* **1987**, S1.
[74] Bruker, Win-EPR SimFonia version 1.26 beta; http://www.bruker-biospin.com/simfonia.html.
[75] J. Peisach, W. E. Blumberg, *Arch. Biochem. Biophys.* **1974**, *165*, 691.
[76] D. Getz, B. L. Silver, *J. Chem. Phys.* **1970**, *52*, 6449.
[77] T. J. Rink, R. Y. Tsien, T. Pozzan, *J. Cell Biol.* **1982**, *95*, 189.
[78] A. M. Paradiso, R. Y. Tsien, T. E. Machen, *Proc. Natl. Acad. Sci. USA* **1984**, *81*, 7436.
[79] R. G. Shulman, T. R. Brown, K. Ugurbil, S. Ogawa, S. M. Cohen, J. A. Den Hollander, *Science* **1979**, *205*, 160.
[80] R. J. Gillies, K. Ugurbil, J. A. Den Hollander, R. G. Shulman, *Proc. Natl. Acad. Sci. USA* **1981**, *78*, 2125.
[81] T. Kalliomaki, R. P. Hill, *Br. J. Cancer* **2004**, *90*, 1842.
[82] R. A. Cairns, T. Kalliomaki, R. P. Hill, *Cancer Res.* **2001**, *61*, 8903.
[83] C. W. Song, R. Griffin, H. J. Park, *Cancer Drug Resistance* (Ed.: B. A. Teicher), Humana press, **2006**, Chapter 2.

[84] S. V. Kozin, P. Shkarin, L. E. Gerweck, *Cancer Res.* **2001**, *61*, 4740.
[85] L. E. Gerweck, S. Vijayappa, S. Kozin, *Mol. Cell. Proteomics Mol. Cancer Therapeut.* **2006**, *5*, 1275.
[86] J. H. Freedman, M. R. Ciriolo, J. Peisach, *J. Biol. Chem.* **1989**, *264*, 5598.
[87] J. R. Turnlund, *Am. J. Clin. Nutr.* **1998**, *67*, 960S.
[88] Y. Fujibayashi, K. Wada, H. Taniuchi, Y. Yonekura, J. Konishi, A. Yokoyama, *Biol. Pharm. Bull.* **1993**, *16*, 146.
[89] H. Okazawa, Y. Yonekura, Y. Fujibayashi, S. Nishizawa, Y. Magata, K. Ishizu, F. Tanaka, T. Tsuchida, N. Tamaki, J. Konishi, *J. Nucl. Med.* **1994**, *35*, 1910.
[90] J. S. Lewis, D. W. McCarthy, T. J. McCarthy, Y. Fujibayashi, M. J. Welch, *J. Nucl. Med.* **1999**, *40*, 177.
[91] P. Hohenberg, W. Kohn, *Phys. Rev.* **1964**, *136*, B864.
[92] W. Kohn, L. J. Sham. *Phys. Rev.* **1965**, *140*, A1133.
[93] Z. Otwinowski, W. Minor, *Methods Enzymol.* **1997**, *276*, 307.
[94] A. Altomare, G. Cascarano, G. Giacovazzo, A. Guagliardi, M. C. Burla, G. Polidori, M. Camalli, *J. Appl. Crystallogr.* **1994**, *27*, 435.
[95] P. W. Betteridge, J. R. Carruthers, R. I. Cooper, K. Prout, D. J. Watkin, *J. Appl. Crystallogr.* **2003**, *36*, 1487.

Received: March 24, 2008
Published online: May 21, 2008

